PROF. STEVE R WILLIAMS (Orcid ID : 0000-0001-5940-1675)

DR. HERVE BOUTIN (Orcid ID : 0000-0002-0029-5246)

Article type : Original Article

Longitudinal investigation of neuroinflammation and metabolite profiles in the APP_{swe}×$PS1_{\Delta e9}$ transgenic mouse model of Alzheimer's disease.

Chaney A.[1,2]*, Bauer M.[3†], Bochicchio D.[2†], Smigova A.[1,2], Kassiou M.[4], Davies K.E.[1], Williams S.R.[1], Boutin H.[1,2].

[1] Centre for Imaging Science, Faculty of Biology, Medicine and Health and Manchester Academic Health Sciences Centre University of Manchester, Manchester, M13 9PT, UK

[2] Wolfson Molecular Imaging Centre, Faculty of Biology, Medicine and Health and Manchester Academic Health Sciences Centre, University of Manchester, Manchester, M20 3LJ, UK.

[3] Medical University Vienna, Department of Clinical Pharmacology, Waehringer Guertel 18-20, 1090 Vienna, Austria.

[4] School of Chemistry, University of Sydney, NSW 2006 Australia.

† Contributed equally to the work

* Current address: 3165 Porter Drive, Stanford University, Palo Alto, CA, 94304.

Corresponding Author:

Dr Hervé Boutin,

Wolfson Molecular Imaging Centre,

27 Palatine Road, Manchester, M20 3LJ, UK

Email: herve.boutin@manchester.ac.uk
Tel: +44 161 275 0078
Fax: +44 161 275 0003

Abstract

There is increasing evidence linking neuroinflammation to many neurological disorders including Alzheimer's disease (AD), however its exact contribution to disease manifestation and/or progression is poorly understood. Therefore, a need exists to find new ways of investigating neuroinflammation in both health and disease. Here we investigate cognitive decline, neuroinflammatory and other pathophysiological changes in the APP_{swe}×$PS1_{\Delta e9}$ transgenic mouse model of AD. Transgenic (TG) mice were compared to C57BL/6 wild type (WT) mice at 6, 12 and 18 months of age. Neuroinflammation was investigated by [^{18}F]DPA-714 positron emission tomography and *myo*-inositol levels using ^{1}H magnetic resonance spectroscopy (MRS) *in vivo*. Neuronal and cellular dysfunction was investigated by looking at N-acetylaspartate (NAA), choline containing compounds, taurine and glutamate also using MRS. Cognitive decline was first observed at 12m-old in the TG mice as assessed by working memory tests. A significant increase in [^{18}F]DPA-714 uptake was seen in the hippocampus and cortex of 18m-old TG mice when compared to age matched WT mice and 6m-old TG mice. No overall effect of gene was seen on metabolite levels; however a significant reduction in NAA was observed in 18m-old TG mice when compared to WT. In addition, age resulted in a decrease in glutamate and an increase in choline levels. Therefore we can conclude that increased neuroinflammation and cognitive decline are observed in TG animals, whereas NAA alterations occurring with age are exacerbated in the TG mice. These results support the role of neuroinflammation and metabolite alteration in AD and in aging.

Key words: Alzheimer's disease, animal model, neuroinflammation, positron emission tomography, magnetic resonance spectroscopy.

Introduction

Alzheimer's disease (AD) is the most common form of dementia which has become a huge socio-economic burden due to an increased aging population. Despite considerable research, the mechanisms leading to its manifestation remain unclear. AD is defined pathologically by amyloid plaques (Aβ), neurofibrillary tangles (NFTs) and neuronal loss (Braak & Braak 1991); however the aetiology remains elusive. Hence, a need exists to find biomarkers that can help understand disease progression and mechanisms, aid diagnosis and track the efficacy of therapeutic interventions.

AD is a multifactorial disease associated with complex neuronal and neuroinflammatory alterations (Heneka *et al.* 2015, Perry & Holmes 2014, Rubio-Perez & Morillas-Ruiz 2012, Mhatre *et al.* 2015, Halliday *et al.* 2000). Activated microglia have been shown to surround amyloid plaques (Haga *et al.* 1989) *ex vivo* and increased inflammatory cytokine expression is observed post-mortem in brain and *in vivo* in the serum and CSF of AD and patients with mild cognitive impairment (MCI) (Varnum & Ikezu 2012, Rubio-Perez & Morillas-Ruiz 2012, Swardfager *et al.* 2010, Forlenza *et al.* 2009, Westin *et al.* 2012). In addition, treatments which experimentally reduce pro-inflammatory cytokines have been shown to improve memory performance (Song *et al.* 2013, Lee *et al.* 2013), suggesting increased inflammation could contribute to memory impairments seen in AD.

The ability to accurately assess neuroinflammation *in vivo* is important to our understanding of the impact it has in AD. The discovery that translocator receptor 18kDa (TSPO) expression is upregulated on activated microglial cells (Papadopoulos *et al.* 2006) has enabled the generation of TSPO radio-ligands to image neuroinflammation *in vivo* using positron emission tomography (PET). TSPO expression in the brain is mainly restricted to endothelial cells and activated microglia, and is low in healthy brain tissue where inflammation is absent (Scarf & Kassiou 2011, Papadopoulos et al. 2006); therefore TSPO PET permits the identification and tracking of region-specific neuroinflammation throughout disease progression. Although it is important to note that TSPO is also expressed endothelial cells and hence in blood vessels (Turkheimer *et al.* 2007).

PK11195, a TSPO ligand, has been successfully labelled with ^{11}C and has shown good correlation to microglial activation *ex vivo* (Venneti *et al.* 2009), however contradictory

reports exist regarding the detection of neuroinflammation in AD using [^{11}C]PK11195 imaging. Some studies have demonstrated increased [^{11}C]PK11195 binding in AD and MCI patients (Edison *et al.* 2008, Yokokura *et al.* 2011), whereas others have reported no differences in any regions between patients and age matched controls (Wiley *et al.* 2009, Schuitemaker *et al.* 2013). Short half-life, low signal to noise ratio, high non-specific binding and modelling issues may have contributed to these contradictory results (Boutin & Pinborg 2015, Varrone & Lammertsma 2015), hence new generation tracers with improved affinities and kinetics such as [^{18}F]DPA-714 (Chauveau *et al.* 2009, Boutin *et al.* 2013, Doorduin *et al.* 2009, James *et al.* 2008) have been developed to assess. Recently, using [^{18}F]DPA-714, Hamelin *et al.* have demonstrated that AD patients with slower cognitive decline had higher level of neuroinflammation (Hamelin *et al.* 2016), hypothesising that neuroinflammation may also exert neuroprotective functions early in the disease. However, this is the first *in vivo* study showing a positive correlation between neuroinflammation and cognitive decline, suggesting a potential beneficial role for neuroinflammation in AD. However this needs to be further investigated as TSPO expression is only a surrogate marker of microglial activation in a broad sense and does not provide information on the functional phenotype of activated microglia. Similarly, TSPO expression has been reported to be increased with ageing (Gulyas *et al.* 2011, Kumar *et al.* 2012) but the role and meaning of this potential increase with age is yet to be fully understood.

Similarly, magnetic resonance spectroscopy (MRS), a method that allows the detection of metabolite profiles *in vivo*, can also be used to investigate neuroinflammation through measurement of myo-inositol (mI) levels. mI has been suggested to be a glial specific marker (Brand *et al.* 1993) indicative of increased gliosis. Although increased levels of mI have been repeatedly reported in AD and MCI subjects in regions associated with degeneration in AD (Parnetti *et al.* 1997, Murray *et al.* 2014, Kantarci 2007, Shinno *et al.* 2007, Shiino *et al.* 2012, Foy *et al.* 2011, Rose *et al.* 1999), evidence suggests that mI does not necessarily correlate with increased microglial activation *ex vivo* (Murray et al. 2014, Pardon *et al.* 2016) and may be more directly associated with plaque load. MRS can also measure other metabolites of interest related to neuronal function including N-acetylaspartate (NAA), glutamate (Glu), taurine (Taur), total choline (tCho) and creatine + phosphocreatine (Cr). NAA is a neuronal marker (Birken & Oldendorf 1989, Urenjak *et al.*

1993) and decreases in its levels are consistently reported in AD patients (Parnetti et al. 1997, Murray et al. 2014, Kantarci 2007, Shinno et al. 2007, Shiino et al. 2012, Foy et al. 2011, Rose et al. 1999, Watanabe *et al.* 2010), suggesting neuronal dysfunction or death. Moreover, mI and NAA levels have been shown to be correlated with Aβ burden (Klunk *et al.* 1992, Murray et al. 2014) and performance in some cognitive tasks (Foy et al. 2011, Rose et al. 1999), implicating both in AD pathology and disease severity.

Although, the majority of AD cases are sporadic, so far most of the animal models use transgenes present in the inheritable familial form. Nevertheless, these models give us insight into the pathological mechanisms underlying AD. Hence, here we used the human double mutation APP_{swe}×$PS1_{\Delta e9}$ mouse model to investigate inflammatory and neuronal integrity biomarkers as indicators of disease progression using MRS, PET, immunohistochemistry and cognitive assessment.

A longitudinal study was conducted in male TG APP_{swe}×$PS1_{\Delta e9}$ and WT C57BL/6 mice to investigate neuroinflammation using PET, neurochemical profile using MRS and cognitive function using several behavioural assessments. This was done with the aim of characterising inflammatory, metabolite and cognitive differences between TG and control animals with age. We hypothesised that there would be increased neuroinflammation (demonstrated by increased DPA-714 uptake and mI levels), neuronal dysfunction (decreased NAA levels), neurotransmitter disturbances (altered Glu) and cognitive decline with age in the TG compared to WT mice.

Methods

Animals

Fourteen TG male APP_{swe}×$PS1_{\Delta e9}$ mice (RRID: MGI:5701399) with a C57BL/6 (RRID: IMSR_JAX:000664) background and 17 WT C57BL/6 mice were acquired from the Jackson laboratory (Bar Harbor, Maine, USA) at 8 weeks of age and allocated to the study. Additionally, 5 WT and 7 TG mice were bred in house and complemented the initial groups (see details below). As the mice are *per se* WT or TG, the WT and TG cannot be randomized. All mice were kept in the Biological Sciences Facility in the University of Manchester. Animals were housed in individually ventilated cages in groups of 2-5 in a 12h:12h light and dark cycle with environmental enrichment and 24h access to food and water. In total, 22

male WT and 21 TG male mice were used in this study. 8 WT and 10 TG were measured repeatedly for MRS (2 WT and 5 TG of these were bred in house); a total of 20 WT and 16 TG (5 WT and 7 TG of these were bred in house) mice were scanned non-repeatedly with PET. This was as a result of 7 TGs and 5 WTs dying of unknown causes or during anaesthesia, and one WT was excluded after abnormal brain morphology was noticed during MR imaging. In addition three animals in each group were used for analysis *ex vivo* at both 6 and 12 months. At 18 months all mice were sacrificed and the brains removed for analysis *ex vivo*. All experiments were carried out in accordance with the Animal Scientific Procedures act 1986 and approved by the University of Manchester Local Ethical Review Committee

Study Design

The study was not pre-registered. Mice underwent longitudinal behavioural testing and imaging (Figure 1) at 6, 12 and 18 months of age (body weights (in grams, mean±SD): 32.9±1.71, 37.9±3.45, 38.9±3.69 in WT and 34.5±3.19, 40.2±4.28, 41.1±6.17 in TG at 6m, 12m, 18m of age respectively). Mice were also tested at 3 (11 WT and 15 TG) and 9 months (9 WT and 12 TG) of age to check for potential changes in behaviour and potentially guide changes in the choice of imaging time-points, however as there was no significant differences between 3, 6 and 9 months' time-points, data from the 3 and 9 months' time-points are not shown here and only the time-points matching the imaging time-points are shown. Imaging experiments began at 6 months of age due to the development of detectable amyloid pathology from this age in this model (Jankowsky *et al.* 2004). Immunohistochemistry was carried out on separate animals at 6 and 12 months (see "animals" above). Animals followed longitudinally were culled and processed for *ex vivo* analysis at 18 months of age. A week gap was given between imaging and behavioural experiments to allow animals to recover from the potential stress of imaging/anaesthesia and limit interference between experiments. All experiments were carried out between 9am and 5pm, with all behaviour carried out between 9am and 2pm for each time-point. For all behavioural tests animals were placed in the testing room 30 minutes prior to experimentation to allow for habituation to the environment.

Behaviour

Novel Object and Smell Recognition Tests

A plastic circular arena (30cm diameter, 21cm height) was used for behavioural testing. Animals were subjected to two days of habituation and one day of novel object recognition (NOR) testing. Habituation involved single mice exploring an empty arena for 5min and was carried out in a random order within the same time-frame each day. NOR utilizes the natural behaviour of rodents to explore novelty to test non-associative working memory (Ennaceur & Delacour 1988). This was assessed by investigating the ability to discriminate between novel and familiar objects and was carried out in both TG and WT mice at 6, 12 and 18 months of age. Small plastic objects of varying shapes and colours (e.g. Lego blocks) were used as NOR objects. Test day consisted of two phases. In phase 1, a mouse was placed in the arena with two identical unfamiliar objects for 10min. After this time, the mouse was returned to its home cage and a 1h delay was implemented. In phase 2, one familiar object was replaced by a novel object and the mouse was given 4min to investigate the objects.

Novel smell recognition (NSR) utilizes the natural exploration of novelty to test working memory in rodents although through olfaction. The experimental design was the same as the NOR, however a 3min delay was implemented and identical plastic scent balls with sniffing holes were stuffed with cotton wool and filled with 0.5ml of a certain scent (e.g. vanilla) were used.

For both the NOR and NSR, behaviour was recorded and analysed retrospectively. In addition, in between trials all objects and areas were cleaned with 70% ethanol to remove any scent of the previous mouse which may alter results.

Time spent investigating left and right identical objects/smells in phase 1 were analysed to assess side bias. Mice were to be excluded if significant side bias (> 60% of time spent investigating one of two identical objects) was observed in phase 1. Time spent exploring the novel and familiar objects in phase 2 was used to generate a discrimination index (DI), defined as the difference between time spent exploring the novel (T_n) and the familiar (T_f) object/scent divided by the total time (T) ($DI=(T_n-T_f)/T$). This resulted in values ranging from -1 to +1. A negative value indicated more time spent with the familiar, a

positive value indicated more time investigating the novel and a zero value indicated no preference.

The re-use of novel objects for each mouse was kept to a minimum to prevent potential memorisation of objects/scents between time-points and ensure the test was unique (i.e. a truly novel object or smell they were never exposed to before). The only exception to this was a small cohort of mice that underwent behavioural testing at 3 months of age to investigate whether early time-points were needed for baseline. No significant differences were observed at this age in this small group and therefore only 6, 12 and 18 months were chosen going forward with behavioural testing.

Y-maze spontaneous alteration task

The Y-maze spontaneous alteration task utilizes the natural exploratory behaviour of rodents to assess spatial learning and short-term memory. The Y-maze test was carried out as described previously shown by Martins et al. (2017). A black Perspex maze with 3 arms (15cm length x 10cm width x 10cm depth per arm) labelled with A-C and with different internal visual cues was used. The mice were placed inside the maze and arm entries were recorded manually over an 8min time period, with entries only valid if the whole body of the mouse entered the arm. Successful spontaneous alternation was defined by consecutive entry into all 3 arms in any order. Analysis was carried out by calculating overlapping triplet sets relative to successful arm entries as previously described (Knight *et al.* 2014, Hiramatsu *et al.* 1997). Percentage of successful alternation was compared between WT and TG mice at all ages.

Behaviour to predator and non-predator urine

A Y maze with either predator or non-predator urine at the end of each arm was used to assess the general olfactory ability of 12-month-old WT and TG mice. The maze had no visual cues. Vented containers were injected with 1ml of bobcat, fox or rabbit urine and were placed at the end of each arm. Mice were allowed to explore the maze for 8min and time (in seconds) spent in each arm was quantified. Time spent in the middle of or rearing on the side of the maze was not counted. Both bobcats and foxes are predators for mice, whereas rabbits are not, hence an increased amount of time in the arm containing rabbit urine would be expected in mice with intact olfaction.

[^{18}F]DPA-714 PET

Neuroinflammation was investigated using the TSPO tracer [^{18}F]DPA-714. [^{18}F]DPA-714 was produced as previously described (James et al. 2008). Animals were anesthetised, cannulated (via tail vein) and injected with [^{18}F]DPA-714 (12.3±1.9MBq). Respiratory rate and temperature were monitored throughout the experiment and body temperature was maintained at 37±0.5^{o}C (BioVet® system m2m Imaging Corp., Cleveland, OH, USA). Images were acquired on a Siemens Inveon® PET-CT scanner using a 60 min dynamic acquisition. CT scans were performed prior to PET acquisition to obtain the attenuation correction map. The time coincidence window was set to 3.432 ns and levels of energy discrimination to 350 keV and 650 keV. List mode data from emission scans were histogrammed into 16 dynamic frames (5×1 min; 5×2 min; 3×5 min and 3×10 min) and emission sinograms were normalised, corrected for attenuation, scattering and radioactivity decay and reconstructed using an OSEM3D protocol (16 subsets and 4 iterations) into images of dimensions 128 (transaxially) ×159 (axially) with 0.776×0.776×0.796 mm voxels. The PET images segmented using the local means analysis method and the organ mean time activity curves were corrected for partial volume effect as previously described (Boutin et al. 2013, Maroy *et al.* 2008, Maroy *et al.* 2010). The correction method combined the geometric transfer matrix (GTM) method and the regions of interest (ROI)-opt method. Dynamic PET images were analysed using Brainvisa and Anatomist software (http://brainvisa.info/web/index.html) and quantified using Waxholm space created by Johnson *et al*. (Johnson *et al.* 2010). This MRI mouse brain template was used to create 3 brain ROIs (all cortical areas & whole hippocampus, subcortical regions and cerebellum) large enough to be accurately quantified based on the spatial resolution of the PET scanner (Supplementary Figure 1a-c). Data are expressed as uptake values normalised to the cerebellum (NUV_{cb}) as previously used in the same mouse model (Serriere *et al.* 2015).

Magnetic Resonance Spectroscopy Acquisition and Analysis

Animals were anesthetised using isoflurane (3% induction and 1-2% maintenance) and medical oxygen at a rate of 2 L/min. Respiratory rate and temperature were monitored throughout the experiments which were conducted using a 7 Tesla magnet connected to a Bruker Avance III console (Bruker Biospin Ltd, UK). An anatomical multi-slice FLASH MRI sequence was used to enable positioning of the hippocampal volume for MRS. Spectra were

acquired using a water-suppressed PRESS sequence (Bottomley 1987) (TR 2500ms, TE 20ms, 512 averages) from a 2.5x4.5x3 mm^3 voxel that covered the hippocampus and the most dorsal part of the thalamus (Supplementary Figure 1d). Prior to acquiring the spectrum the localized voxel was shimmed using 'FASTMAP' (Gruetter 1993) and water suppression was optimized using VAPOR (Griffey & Flamig 1990). A non-water-suppressed reference PRESS spectrum was also acquired (1 average).

A metabolite basis-set was simulated using NMRScope with the same spectroscopic parameters used for the PRESS acquisition (jMRUI version 5) (Stefan *et al.* 2009). Metabolites included in the basis-set were: NAA, Glu, mI, Cre, GABA, scyllo-inositol (Scy-I), Gln, Tau and tCho. Peaks at 0.9 and 1.3ppm were included to model lipid/macro-molecules. Another additional peak was added at 3.76ppm to cover the detection of α-protons of amino acids (AAP) not otherwise included in the basis set. These additional peaks were added to help with spectral fitting as significant residual signal had previously been found at these resonances (Forster *et al.* 2013). An example of an *in vivo* spectrum with labelled metabolites is shown in supplementary Figure 1e. Spectra were pre-processed by applying a HLSVD (Hankel Lanczos Singular Values Decomposition) filter to supress the residual water signal (van den Boogaart *et al.* 1994). Metabolite concentration *in vivo* was measured using the jMRUI version 5 algorithm QUEST (Ratiney *et al.* 2005). QUEST compiles the metabolite theoretical signals into a basis-set, and then fits the signals to the spectra *in vivo*, allowing detection and measurement. QUEST was run without background handling. Results were referenced to Cr. Referenced data was used to compare metabolite levels in WT compared to TG mice.

Tissue Collection and Immunohistochemistry

Immunohistochemistry was carried out on TG and WT animals (n=3-5) to visualise CD11b (microglial marker), GFAP (astroctyic marker), TSPO, 6E10 (Aβ marker), SVA2 (synaptic vesicle marker), MAP2 (microtubule marker) and NeuN (neuronal marker). Animals were culled by isoflurane overdose confirmed by cervical dislocation. The brains were collected, snap frozen using isopentane on dry ice and stored at -80°C. Coronal brain sections (20µm thick), from the rostral to caudal part of the brain, were taken using a cryostat (Leica CM3050s, Leica Biosystems Nussloch GmbH, Germany) and stored at -80°C. Sections were allowed to defrost and dry at room temperature for 20min and then fixed

with 4% paraformaldehyde for 10min before being washed (6×5min) in phosphate buffered saline (PBS) and incubated for 30 minutes in 2% normal donkey serum and 0.1% Triton X-100 in PBS to permeabilize and block non-specific binding. TSPO, 6E10, SV2A and neurogranin immunohistochemistry required an extra step of antigen retrieval done by incubating the slides in 10mM citrate buffer at 90°C for 20min and then washed 2×3 min in PBS. Primary antibody incubation was carried out overnight at 4°C with one of the following primary antibodies in 2% normal donkey serum and 0.1% Triton X-100 in PBS: rat anti-mouse CD11b (AbD Serotec (MCA711), RRID: AB_321292, 1:1000); rabbit anti-mouse TSPO (Abcam (EPR5384), RRID: AB_10862345, 1:250); rabbit anti-mouse GFAP (DAKO (Z0334), RRID: AB_10013382, 1:1000); mouse anti-human 6E10 amyloid (BioLegend (803001), RRID: AB_2564653, 1:1000); rabbit anti-mouse SV2A (Abcam (ab32942), RRID: AB_778192, 1:500); chicken anti-mouse MAP2 (Abcam (ab5392), RRID: AB_2138153, 1:1000); rabbit anti-mouse NeuN (Abcam (ab177487), RRID: AB_2532109, 1:500); rabbit anti-mouse Neurogranin (Abcam (ab23570), RRID: AB_447526, 1:500). Following incubation in primary antibody, PBS washes were repeated (3×10min) and incubated with one of the following secondary antibodies was carried out: Alexa Fluor 594nm Donkey anti-rat IgG 1:500 (for CD11b); Alexa Fluor 488nm Donkey anti-rabbit IgG 1:500 (for TSPO, GFAP, SV2A); Alexa Fluor 594nm Donkey anti-mouse IgG 1:500 (for 6E10); Alexa Fluor 488nm Goat anti-chicken Double staining was carried out for CD11b+TSPO, CD11b+GFAP and 6E10+TSPO and to allow the visualisation of microglia and astrocytes with TSPO expression and Aβ burden. Double staining was also carried out for MAP2+NeuN to look at neuronal density.

Images of the hippocampus and cortex were collected between bregma -2.06mm and -2.30mm on an Olympus BX51 upright microscope using a 10×/0.30 or 20×/0.50 UPlanFLN objectives and captured using a Retiga 6000 Color camera through QCapture Pro 7 Software (QImaging Inc.). Specific band pass filter sets were used to prevent bleed through from one channel to the next.

Statistical analysis

No blinding *stricto sensu* was performed, however animals were identified and recorded only using a unique code number during behavioural tests and image analysis and only identified as TG or WT post-analysis so that the observers could not know whether the animal being analysed was a WT or a TG. Sample size were calculated to n=9-10 per group

using anterior data obtained in our laboratory using the following online tool: https://www.stat.ubc.ca/~rollin/stats/ssize/n2.html (with α=0.05, β=0.2, with anticipated mean difference of 8% and SD~5-8%).

The data were statistically analysed using GraphPad Prism version 5.04. Behavioural data are expressed as mean±SEM and imaging data are expressed as mean±SD. Paired *t* tests were used to determine differences in exploration in phase 1 of both the NOR and NSR tests. Two way analysis of variance (ANOVA) were carried out to test the effect of strain and age on DI, percentage of successful alternation in the Y-maze, metabolite levels and [^{18}F]DPA-714 uptake in WT and TG mice. Post-hoc analysis was carried out using Dunnet's and Sidak's tests. Main effects were considered significant if $p \leq 0.05$. Interactions were deemed significant if $p \leq 0.1$. Significance was not adjusted for comparisons of multiple region of interest as those were not compared between them, but if a Bonferoni correction had been applied to the DPA-714 to account for the number of regions analysed, the appropriate adjusted P value would be $P<0.017$.

Results

TG mice display increased cognitive decline

To test whether short-term working and recognition memory were affected at different ages, Y maze and novel recognition tests were carried out (Figure 2). No significant differences in DI were seen between WT and TG mice in the NOR at 6 months of age (Figure 2a). Both groups displayed positive DI results suggesting a preference for the novel and indicating good short-term memory at this age. However, analysis revealed a significant interaction between gene and age (Figure 2a, p=0.0225). This effect was due to a significant decrease in cognitive performance in the TG mice compared to the WT mice at 12 months of age as assessed by DI scores ($p \leq 0.01$). This effect was not replicated at 18 months of age, whereby both groups displayed low DI scores suggesting poor cognitive performance in both WT and TG by this age. No significant differences were seen in the exploration of identical objects in phase 1 of the NOR (Figure 2b) indicating that there was no side bias in the test.

No significant differences in performance were seen between groups in the NSR (Figure 2c). At 6 months of age, both WT and TG were able to discriminate between novel

and familiar smell, demonstrating good working memory and olfaction. Although no side bias was observed in phase 1 (Figure 2d), high variation was seen in this test from 12 months of age onwards, therefore the olfactory ability of these mice was tested at this age. In the olfaction test the behaviour to predator and non-predator urine was tested. Neither WT nor TG spent significantly more time in the arms containing rabbit urine when compared to fox or bobcat urine (Figure 2e) indicating olfactory dysfunction from 12 months of age.

TG mice also displayed increased cognitive decline in the Y-maze test (Figure 2f). Overall decreased percentages of successful alternation were seen in the TG mice as an effect of gene ($p=0.0001$). In addition, a significant interaction was observed between gene and age ($p=0.0233$). This effect did not reveal any significant differences in Y-maze performance at 6 or 12 months of age. In contrast, at 18 months a significant decrease in the percentage of alternation was observed in TG mice compared to age matched WT mice ($p\leq0.001$) indicating accelerated decline in short-term working memory in TGs at this age.

[^{18}F]DPA-714 binding significantly increases *in vivo* as a result of AD-like pathology and age

To assess neuroinflammation differences between APP_{swe}×$PS1_{\Delta e9}$ and WT mice, [^{18}F]DPA-714 NUV_{cb} was compared at 6, 12 and 18 months in the hippocampal+cortical and subcortical ROIs (Figure 3a). Statistical analysis of the cerebellum standard uptake value (SUV) revealed a significant effect of age only, which the Sidak's post-hoc test revealed to be between 6 and 18 months old WT only. No other difference, particularly between WT and TG, could be found in the cerebellum SUV justifying the use of the cerebellum to normalise the uptake values as previously done in this type of study (Serriere *et al.* 2015, Takkinen *et al.* 2016). A two-way ANOVA revealed a significant effects of gene ($p=0.02$) and age ($p=0.03$) on [^{18}F]DPA-714 uptake in the hippocampus and cortex, which resulted in a modest but significant increase in [^{18}F]DPA-714 NUV_{cb} uptake in TG mice at 18 months of age (0.930±0.059) when compared to both age-matched WT (Figure 3b, 0.870±0.044; +7%, $p=0.04$) and 6-month-old TG mice (0.866±0.051; +7%, $p=0.03$). These results suggest that both age and disease increase the neuroinflammatory status of TG mice. An increasing effect was seen with age on [^{18}F]DPA-714 NUV_{cb} values in the other subcortical region ($p=0.0008$) and a significant increase in [^{18}F]DPA-714 NUV_{cb} uptake was seen in other subcortical regions of 18 months old TG mice (0.638±0.034) when compared to 6 months

old TG mice (Figure 3b, 0.726±0.067; +14%, p=0.002). The same trend was observed in the subcortical regions of WTs but was not significant (**Error! Reference source not found.**Figure 3c, p=0.058).

Metabolite profiles of APP_{swe}×$PS1_{\Delta e9}$ and WTs are affected by age

Single voxel ^{1}H MRS was repeated in the same cohort of TG and WT mice at 6, 12 and 18 months of age to investigate changes in metabolite profile. A 3×3×3 mm voxel was placed to encompass the hippocampus and the most dorsal part of the thalamus. Example spectra from this region can be seen in Figure 4a. No significant differences were seen in Cr concentration referenced to water at any age group for either WT or TG mice (Figure 4d), allowing metabolite data to be expressed as a ratio to Cr. This has been previously reported in this model (Jansen *et al.* 2013), however it was important to assess this as elevated Cr levels, compared to WT mice, have previously been reported in the TASTPM mouse model of AD *in vivo* at an early age (Forster *et al.* 2013) and at a later age analysing brain extracts *in vitro* (Forster *et al.* 2012). No overall significant effects of gene were seen on any metabolite in these animals. However, a significant effect of age (p=0.0006) and a significant interaction between gene and age (p=0.0866) was observed for NAA. This effect resulted in significantly lower NAA in 18-month-old TG mice compared to 6-month-old TG mice using multi-comparisons analysis (-58%, Figure 4b, p≤0.0001). This aging effect was seen in the WT mice (-20%) but was not statistically significant. Significant aging effects were also observed on Glu (p=0.0003) and tCho (p=0.0016) levels, resulting in reduced Glu (-53% average across groups from 6 to 18 months) and increased tCho (+71% average across groups from 6 to 18 months) levels with age. No gene effect or gene×genotype interaction was associated with these changes suggesting that these alterations are an effect of normal aging.

Immunohistochemistry

To verify the *in vivo* imaging results, e*x vivo* immunohistochemistry was performed to assess the presence of neuroinflammation, Aβ burden and neuronal integrity. GFAP and CD11b positive staining was seen in the hippocampus (Figure 5a) and cortex (Figure 5b) of TG mice but not WT mice. Low levels of immunostaining were evident at 6 months of age and increased with age in both regions in TG mice. Similarly, double staining for TSPO and CD11b revealed an increase in both proteins with age in the hippocampus (Figure 6a) and cortex (Figure 6b) of the TG mice. In the TG mice, there was regional co-expression of TSPO

and CD11b in the hippocampus and cortex, with a modest expression at 6 months of age increasing at 12 months and further at 18 months. In WT animals, TSPO staining was only seen in the vessels and not the parenchyma in both regions. No CD11b staining was evident in the WTs at any age. Immunostaining for TSPO and Aβ pathology (6E10) revealed similar results. An age dependent increase was seen in Aβ burden in both the hippocampus (Figure 7a) and cortex (Figure 7b) of TG mice only. Aβ staining was sparse at 6 months but increased with age revealing a heavy burden by 18 months. CD11b, TSPO and 6E10 demonstrated good regional co-expression from 6 to 18 months in the cortex of TG mice, indicating increased microglial activation around Aβ plaques. No Aβ staining was evident in the WT mice at any age. No differences were seen in staining for MAP2, NeuN (Figure 8a-b) and SV2A and neurogranin (Figure 9a-b) between TG and WT mice or with age in the hippocampus or cortex indicating that neuronal death could not be detected in this model with this method.

Discussion

In vivo studies

Cognitive performance in the TG group at 6 months of age was comparable to WT mice and has been previously reported in a variety of memory based tests in this (Chen *et al.* 2012, Jansen et al. 2013) and other AD models (Webster *et al.* 2013, Nagakura *et al.* 2013). This supports the low levels of Aβ load observed at this age in this and other studies (Jankowsky et al. 2004, Garcia-Alloza *et al.* 2006). TG mice displayed deficits in non-associative recognition memory and working memory from 12 months, with reduced cognitive performance in the NOR test and Y maze by 12 and 18 months respectively. Cognitive deficits in these tests have been previously reported in both this (Petrov *et al.* 2015) and other amyloid based models of AD (Martins et al. 2017, Daniels *et al.* 2016, Forster et al. 2013), further supporting the link between pathology burden and cognitive decline. WT mice retained memory later in both tests, displaying increased working memory in the Y-maze test compared to TG at 18 months. However, no differences in cognition were identified in the NSR test. Both WT and TG were able to discriminate between novel and familiar scents at 6 months of age, demonstrating good working memory and olfaction. However, high variation in both groups was observed in this test from 12 months onward, therefore we hypothesised that these animals may have altered olfaction by this age, which

was proven by the lack of preference of exposure to non-predator (rabbit) urine over predator (bobcat and fox) urine. An increased amount of time in the arm with non-predator urine would be expected in mice with intact olfaction; hence this result suggests may be down to reduced olfaction rather than cognitive deficit. These results are in part in line with previous publications showing various alterations of olfaction in Tg2576 (Wesson *et al.* 2011) and in APP_{swe}×$PS1_{\Delta e9}$ mice (Yao *et al.* 2016) using different tests and with clinical reports showing that loss of olfaction is common in neurodegenerative diseases and is an early sign of AD (Mesholam *et al.* 1998). We however also observed a loss of olfaction in our WT mice. Similarly, some previous studies reported early cognitive dysfunction prior to pathology development using different behavioural assessments such as the Morris water maze (Zhang *et al.* 2012). Here we report decline in memory with age in APP_{swe}×$PS1_{\Delta e9}$ mice, which is in support of our working hypothesis that cognitive performance decreases with age at a faster rate in the TG mice compared to the WT.

It has been hypothesized that neuroinflammation precedes clinical manifestation of cognitive dysfunction in AD. In this study, we observed the presence of neuroinflammation in TG mice via immunohistochemistry (CD11b and GFAP) from 6 months which increased with age. However, increased neuroinflammation and altered metabolite profile, assessed via *in vivo* PET and MRS respectively, occurred after the emergence of cognitive decline in this animal model.

Increased [^{18}F]DPA-714 NUV_{cb} was found in the hippocampal and cortical region of old TG mice when compared to both age matched WT mice and young TG mice, suggesting that increased neuroinflammation in hippocampal and cortical region is driven by the presence of AD pathology in TG mice. This increase was only statistically significant at 18 months of age despite increased Aβ, GFAP and CD11b immunostaining evident from 12 months of age. Although a significant increase is also seen with age in [^{18}F]DPA-714 uptake in the other subcortical regions, no significant differences were found between genotypes. A trend towards significance was also observed in the WTs in the subcortical ROI. As these regions have little to no amyloid burden, these data suggest that neuroinflammation in these regions is increased mostly as a result of normal aging and independently of amyloid pathology. It is however notable that Yokokura *et al.* recently reported increased uptake in the thalamus of AD and elderly patients using [^{11}C]DPA-713 (Yokokura *et al.* 2017). These

results suggest that neuroinflammation is present prior to cognitive dysfunction, however current *in vivo* methods are not sensitive enough (due to a combination of tracer sensitivity, resolution capabilities of small animal PET and non-specific relevance of the mI signal) to detect the more subtle inflammatory changes in the earlier stages of disease that are achievable via *ex vivo* methods.

Our data are in agreement with previous reports in mouse models using [^{18}F]DPA-714. Serriere *et al.* investigated [^{18}F]DPA-714 uptake in the same mouse model at 6, 9, 12, 15 and 19 months of age (Serriere *et al.* 2015). NUV_{Cb} were increased in the cortex of TG mice at 12 and 19 months (but not 15 months of age) and in the hippocampus at 19 months of age. Increased cortical [^{18}F]DPA-714 NUV_{cb} has also been reported in the APP/PS1-21 mouse from 6 months of age, with hippocampal increases emerging from 12 months of age (Takkinen *et al.* 2016). In our analysis methods, we pooled cortical and hippocampal areas as one region due to AD pathology present in both regions and because the size of the pooled ROI is more realistically compatible with the resolution of PET imaging in preclinical scanners (~1-1.6mm). Therefore, by pooling the hippocampus and cortex into a single ROI, we may have masked the possible differential time-effect between each region, and hidden the earlier increase in neuroinflammation in the cortex. However, such difference would be small as our immunohistochemistry results show only a slightly stronger signal in CD11b and TSPO in the cortex than in the hippocampus in this model at 6 and 12 months of age. On the other hand, it can also be argued that thin ROIs including only the cortical hippocampal areas (~1.5mm thick) are far more subject to partial volume effects, which could consequently have biased the quantification in previous studies. A significant effect of both age and gene on TSPO PET has been also recently reported in the same model using [^{18}F]GE-180 (Liu *et al.* 2015). Increased [^{18}F]GE-180 uptake was seen in the hippocampus of old TGs compared to age matched WTs and young TG and WT mice. In addition, increased [^{18}F]GE-180 uptake was also seen in the whole brain of old TGs compared to young TGs. This age effect was replicated in WT mice with significant increases in uptake from young to old mice in both hippocampal and whole brain, implicating both normal aging and AD pathology on neuroinflammatory status. Increased neuroinflammation has also been observed as an effect of aging in both humans (Kumar et al. 2012, Yokokura et al. 2017, Gulyas et al. 2011) and in the WTs of other AD models (Brendel *et al.* 2016). Altogether, our results further

support previous findings that age can significantly alter microglial responses, which are modified further in the presence of neurodegenerative diseases such as AD. Increases in TSPO expression have been found in other models of AD (James *et al.* 2015, Brendel *et al.* 2016, Ji *et al.* 2008, Mirzaei *et al.* 2016) and in human AD (Varnum & Ikezu 2012, Rubio-Perez & Morillas-Ruiz 2012, Swardfager et al. 2010, Forlenza *et al.* 2009), indicating that elevated neuroinflammation is a consistent characteristic of this disease. The modest increases and the relative overlap between WT and TG mice demonstrated by the present data and others' are also in agreement with the PET quantification in AD patient vs healthy controls which generally reports non-significant (Varrone *et al.* 2013) or small to more substantial increases (+10-35%) (Schuitemaker *et al.* 2013, Hamelin *et al.* 2016, Okello *et al.* 2009, Edison *et al.* 2008, Varrone *et al.* 2015) in neuroinflammation. This demonstrates that *i)* measuring neuroinflammation *in vivo* in AD is challenging because the amplitudes of changes are overall modest when compared with the changes induced by ageing only and *ii)* that, at least from this point of view, animal models are actually reflecting the clinical situation quite well. Finally, a recent study by Owen *et al.* (Owen *et al.* 2017) suggests that, at least in human, TSPO expression may reflect microglia density rather than microglia phenotype. Although obtained from a purely *in vitro* setting in which cells may behave differently than in their *in vivo* environment, these observations taken together with the known TSPO expression by endothelial cells may explain the inconsistencies between imaging studies and the difficulties encountered over the years to truly assess microglial activation in AD patients using TSPO PET.

In contrast to increased neuroinflammation assessed by PET and immunohistochemistry, no alterations in mI levels were observed between TG and WT mice in this study. This lack of agreement between neuroinflammatory status and mI expression questions the role of mI as a putative marker for gliosis with the specific biological significance of mI needing further investigation to be truly elucidated. In support of this, reported mI level alterations are inconsistent in this model, with both increased and stable levels reported (von Kienlin *et al.* 2005, Dedeoglu *et al.* 2004, Jansen et al. 2013). Moreover, in a clinical study mI was found to be associated with amyloid pathology and not neuroinflammation (Murray *et al.* 2014), therefore it is possible that mI levels represent more closely amyloid load than neuroinflammation. On the other hand we have extensive

amyloid burden in this model without seeing mI alterations. These results are in contrast to many other reports demonstrating increased mI levels in clinical AD (Foy *et al.* 2011, Shiino *et al.* 2012, Murray *et al.* 2014, Kantarci *et al.* 2007, Shinno *et al.* 2007) and AD models (Chen *et al.* 2009, Chen et al. 2012, Marjanska *et al.* 2005, Jack *et al.* 2007, Oberg *et al.* 2008, Choi *et al.* 2014, Choi *et al.* 2010, Marjanska *et al.* 2014, Yang *et al.* 2011, Forster et al. 2013). Chen *et al.* reported significantly higher mI/Cr levels in the APP_{swe}×$PS1_{\Delta e9}$ compared to WT mice as early as 3 months of age (Chen *et al.* 2009). However the voxel used in this study included cortical as well as hippocampal tissue. Here we report the appearance of inflammation and plaques in cortical regions prior to and more frequently than in hippocampal regions, so the discrepancies between studies might be due to differences in size and location of the voxel used as well as the age studied.

Although no qualitative changes were observable in neuronal markers (MAP2 and NeuN) using immunohistochemistry, a significant effect of aging and a significant genotype×age interaction was observed on NAA levels, resulting in a -58% decrease in NAA/Cr in 18 months old TG mice when compared to 6 months old TG. This effect was not mirrored in the WT mice and suggests that decreased NAA levels, although influenced by both age and gene, are slightly more pronounced in TG mice. This underlines the importance of understanding the pattern of normal aging within brain metabolites or other potential biomarkers and the possible confounding effects of age.

Chen *et al.* reported a small but significant decrease (-11% change, 1.16±0.07 in WT vs 1.03±0.06 in TG) in NAA/Cr from 5 months of age (Chen et al. 2009). In contrast, we report NAA alterations post-cognitive decline and is in line with the results from Xu *et al.* in the same animal model (Xu *et al.* 2010). Xu *et al.* found a significant decrease in hippocampal NAA/Cr in 16 month APP_{swe}×$PS1_{\Delta e9}$ TG mice compared to younger TG mice, which was not seen in WT mice. Similar decreases in NAA/Cr associated with age and AD pathology have been reported in other models of AD, at varying ages (Jansen et al. 2013, Xu et al. 2010, Jack et al. 2007, Forster et al. 2013, Choi et al. 2010, Oberg et al. 2008, Marjanska et al. 2005, Choi et al. 2014). We also report age to have a significant effect on Glu and tCho levels without an effect of genotype effect or an interaction genotype×age, in which Glu levels were decreased and tCho levels increased in both WT and TG mice. Similarly, specific reduced Glu and increased tCho levels have been reported in mouse

models of AD (Marjanska et al. 2005, Jack et al. 2007, Chen et al. 2012, Oberg et al. 2008, Dedeoglu et al. 2004, Choi et al. 2010, von Kienlin et al. 2005, Esteras *et al.* 2012) and in the clinical situation (Shiino et al. 2012, Hattori *et al.* 2002, Kantarci 2007, Foy et al. 2011, Griffith *et al.* 2008) vs WT or healthy controls respectively. This result suggests that these effects are a result of normal aging in this strain.

Ex vivo immunohistochemistry

To verify the *in vivo* imaging results, e*x vivo* immunohistochemistry was performed to assess the presence of microglia, astrocytes, TSPO expression and Aβ pathology. Aβ pathology was sparse in young TG mice with increasing burden evident by 12 months and abundant plaques by 18 months. This level of Aβ burden is line with many previous reports in this model (Garcia-Alloza *et al.* 2006, Jankowsky *et al.* 2004, van Groen *et al.* 2006). Similarly, low levels of CD11b, GFAP and TSPO staining were evident in the hippocampus and cortex of TG mice at 6 months, which increased with age. Co-localisation of CD11b and TSPO was observed in the cortex and the hippocampus, confirming that in this model TSPO is mostly expressed by microglia. Similarly, TSPO and Aβ co-localisation was observed in the cortex of TG mice, indicating increased glial activation around Aβ plaques. Similarly, strong astrogliosis was detected around microglial cells which were found only around Aβ plaques supporting the presence of both astrocytes and microglia around Aβ plaques. Microglial cells are known to surround plaques in human AD and have been shown to co-localize with pathology in AD models further supporting the role of neuroinflammation in AD. In contrast to our results, Ji *et al.,* did not find co-expression of CD11b and TSPO in the APP23 mouse model, but found co-localisation of GFAP and TSPO which were in close proximity to amyloid plaque staining (Ji *et al.* 2008). Whereas the opposite was identified in a tau model, with CD11b but not GFAP positive cells expressing TSPO. These results suggest that different forms of tau and amyloid pathology may alter TSPO expression differently *in vivo* (Jansen *et al.* 2013). This may be due to potential differences in type of amyloid, aggregation properties, expression levels, and age of pathology emergence between different models of AD, which may differently affect the glial response (Stalder *et al.* 1999, Xiong *et al.* 2011, Huang *et al.* 2016). In contrast, TSPO expression was only visible in the vessels in WT animals which are in agreement with previous report demonstrating the expression of TSPO in vessels (Turkheimer et al. 2007).

We did not identify any striking reductions in neuronal, synaptic vesicle or microtubule markers in this study. This is in line with previous reports (Jansen *et al.* 2013) suggesting that APP mutations are not sufficient to cause neuronal loss that is observed in human AD and models with tau abnormalities but in contrast with Huang *et al.* who reported a decrease (~20%) in NeuN staining and hippocampal atrophy (~20-30%) (Huang *et al.* 2016). On the other hand amyloid pathology induced cognitive decline and resulted in accelerated NAA loss with age in TG compared to WT mice. This lack of congruency could be explained by many factors such as assessing the wrong neuronal/synaptic markers, changes being too small or regionally specific or as a result of changes in certain neuronal populations (e.g cholinergic) to be detectable using the methods and markers used here.

Conclusion

It has become evident that Alzheimer's disease is a complex multi-factorial disease in which neuroinflammation plays a pivotal role. In support of this, we report increased neuroinflammation in the form of increased [^{18}F]DPA-714 uptake, confirmed through the use of immunohistochemistry, and reduced neuronal function in the form of accelerated NAA reductions in the APP_{swe}×$PS1_{\Delta e9}$ similar to those measured in AD patients. We here show that TSPO PET can detect changes in neuroinflammation in this mouse model, however not as early as detected using *ex vivo* techniques. This suggests that, although TSPO PET is a viable imaging technique to study AD in animal models, the current restrictions due to resolution and brain size in mice hamper earlier detection. Moving to larger species such as rats may address this. Overall, these results support the role of neuroinflammation in the pathogenesis of AD and the potential use of metabolite alteration to monitor disease progression or response to treatments.

Acknowledgements

MK generously provided the precursor and cold reference for the production of [^{18}F]DPA-714. HB was the grant holder of the European Union's Seventh Framework Programme (FP7/2007-2013) under grant agreement n°HEALTH-F2-2011-278850 (INMiND) which funded this work.

The MR facility was supported through an equipment grant from BBSRC UK (BB/F011350). The developers of jMRUI (Stefan et al. 2009) and the support of it through

the EU FP7 'TRANSACT' (FP7-PEOPLE-2012-ITN- 316679) are hereby acknowledged. The authors also wish to thank all the personnel of the WMIC, especially Dr Michael Fairclough, Ms. Lidan Christie, Mr Michael Green, Mr Jamil Gregory, Ms Carol Brough and Ms Gemma Chapman for facilitating the study. We would also like to thank Drs Jack-Auty and Rebecca Montacute who helped with the breeding of some of the mice used in this study.

Conflicts of Interest

All authors report no conflict of interest.

References

Birken, D. L. and Oldendorf, W. H. (1989) N-acetyl-L-aspartic acid: a literature review of a compound prominent in 1H-NMR spectroscopic studies of brain. *Neurosci Biobehav Rev*, **13,** 23-31.

Bottomley, P. A. (1987) Spatial localization in NMR spectroscopy in vivo. *Annals of the New York Academy of Sciences*, **508,** 333-348.

Boutin, H. and Pinborg, L. H. (2015) TSPO imaging in stroke: from animal models to human subjects. *Clinical Translational Imaging*, **3,** 423-435.

Boutin, H., Prenant, C., Maroy, R. et al. (2013) [^{18}F]DPA-714: direct comparison with [^{11}C]PK11195 in a model of cerebral ischemia in rats. *PLoS One*, **8,** e56441.

Braak, H. and Braak, E. (1991) Neuropathological stageing of Alzheimer-related changes. *Acta Neuropathol*, **82,** 239-259.

Brand, A., Richter-Landsberg, C. and Leibfritz, D. (1993) Multinuclear NMR studies on the energy metabolism of glial and neuronal cells. *Dev Neurosci*, **15,** 289-298.

Brendel, M., Probst, F., Jaworska, A. et al. (2016) Glial Activation and Glucose Metabolism in a Transgenic Amyloid Mouse Model: A Triple-Tracer PET Study. *J Nucl Med*, **57,** 954-960.

Chauveau, F., Van Camp, N., Dolle, F. et al. (2009) Comparative evaluation of the translocator protein radioligands 11C-DPA-713, 18F-DPA-714, and 11C-PK11195 in a rat model of acute neuroinflammation. *J Nucl Med*, **50,** 468-476.

Chen, S. Q., Cai, Q., Shen, Y. Y., Wang, P. J., Teng, G. J., Zhang, W. and Zang, F. C. (2012) Age-related changes in brain metabolites and cognitive function in APP/PS1 transgenic mice. *Behav Brain Res*, **235,** 1-6.

Chen, S. Q., Wang, P. J., Ten, G. J., Zhan, W., Li, M. H. and Zang, F. C. (2009) Role of myo-inositol by magnetic resonance spectroscopy in early diagnosis of Alzheimer's disease in APP/PS1 transgenic mice. *Dement Geriatr Cogn Disord*, **28,** 558-566.

Choi, J. K., Carreras, I., Aytan, N., Jenkins-Sahlin, E., Dedeoglu, A. and Jenkins, B. G. (2014) The effects of aging, housing and ibuprofen treatment on brain neurochemistry in a triple transgene Alzheimer's disease mouse model using magnetic resonance spectroscopy and imaging. *Brain Res*, **1590,** 85-96.

Choi, J. K., Jenkins, B. G., Carreras, I., Kaymakcalan, S., Cormier, K., Kowall, N. W. and Dedeoglu, A. (2010) Anti-inflammatory treatment in AD mice protects against neuronal pathology. *Exp Neurol*, **223,** 377-384.

Daniels, M. J., Rivers-Auty, J., Schilling, T. et al. (2016) Fenamate NSAIDs inhibit the NLRP3 inflammasome and protect against Alzheimer's disease in rodent models. *Nat Commun*, **7,** 12504.

Dedeoglu, A., Choi, J. K., Cormier, K., Kowall, N. W. and Jenkins, B. G. (2004) Magnetic resonance spectroscopic analysis of Alzheimer's disease mouse brain that express mutant human APP shows altered neurochemical profile. *Brain Res,* **1012,** 60-65.

Doorduin, J., Klein, H. C., Dierckx, R. A., James, M., Kassiou, M. and de Vries, E. F. (2009) [11C]-DPA-713 and [18F]-DPA-714 as new PET tracers for TSPO: a comparison with [11C]-(R)-PK11195 in a rat model of herpes encephalitis. *Mol. Imaging Biol.,* **11,** 386-398.

Edison, P., Archer, H. A., Gerhard, A. et al. (2008) Microglia, amyloid, and cognition in Alzheimer's disease: An [11C](R)PK11195-PET and [11C]PIB-PET study. *Neurobiol. Dis.,* **32,** 412-419.

Ennaceur, A. and Delacour, J. (1988) A new one-trial test for neurobiological studies of memory in rats. 1: Behavioral data. *Behav Brain Res,* **31,** 47-59.

Esteras, N., Alquezar, C., Bartolome, F., Antequera, D., Barrios, L., Carro, E., Cerdan, S. and Martin-Requero, A. (2012) Systematic evaluation of magnetic resonance imaging and spectroscopy techniques for imaging a transgenic model of Alzheimer's disease (AbetaPP/PS1). *J Alzheimers Dis,* **30,** 337-353.

Forlenza, O. V., Diniz, B. S., Talib, L. L., Mendonca, V. A., Ojopi, E. B., Gattaz, W. F. and Teixeira, A. L. (2009) Increased serum IL-1beta level in Alzheimer's disease and mild cognitive impairment. *Dement. Geriatr. Cogn. Disord.,* **28,** 507-512.

Forster, D., Davies, K. and Williams, S. (2013) Magnetic resonance spectroscopy in vivo of neurochemicals in a transgenic model of Alzheimer's disease: a longitudinal study of metabolites, relaxation time, and behavioral analysis in TASTPM and wild-type mice. *Magn Reson Med,* **69,** 944-955.

Forster, D. M., James, M. F. and Williams, S. R. (2012) Effects of Alzheimer's disease transgenes on neurochemical expression in the mouse brain determined by (1)H MRS in vitro. *NMR Biomed,* **25,** 52-58.

Foy, C. M., Daly, E. M., Glover, A., O'Gorman, R., Simmons, A., Murphy, D. G. and Lovestone, S. (2011) Hippocampal proton MR spectroscopy in early Alzheimer's disease and mild cognitive impairment. *Brain topography,* **24,** 316-322.

Garcia-Alloza, M., Robbins, E. M., Zhang-Nunes, S. X. et al. (2006) Characterization of amyloid deposition in the APPswe/PS1dE9 mouse model of Alzheimer disease. *Neurobiol Dis,* **24,** 516-524.

Griffey, R. H. and Flamig, D. P. (1990) VAPOR for Solvent-Supressed, Short-Echo, Volume-Localized Proton Spectroscopy. *Journal of Magnetic Resonance,* **88,** 161-166.

Griffith, H. R., den Hollander, J. A., Okonkwo, O. C., O'Brien, T., Watts, R. L. and Marson, D. C. (2008) Brain metabolism differs in Alzheimer's disease and Parkinson's disease dementia. *Alzheimer's & dementia : the journal of the Alzheimer's Association,* **4,** 421-427.

Gruetter, R. (1993) Automatic, localized in vivo adjustment of all first- and second-order shim coils. *Magn Reson Med,* **29,** 804-811.

Gulyas, B., Vas, A., Toth, M., Takano, A., Varrone, A., Cselenyi, Z., Schain, M., Mattsson, P. and Halldin, C. (2011) Age and disease related changes in the translocator protein (TSPO) system in the human brain: positron emission tomography measurements with [11C]vinpocetine. *Neuroimage,* **56,** 1111-1121.

Haga, S., Akai, K. and Ishii, T. (1989) Demonstration of Microglial Cells in and around Senile (Neuritic) Plaques in the Alzheimer Brain - an Immunohistochemical Study Using a Novel Monoclonal-Antibody. *Acta Neuropathologica,* **77,** 569-575.

Halliday, G., Robinson, S. R., Shepherd, C. and Kril, J. (2000) Alzheimer's disease and inflammation: a review of cellular and therapeutic mechanisms. *Clin Exp Pharmacol Physiol,* **27,** 1-8.

Hamelin, L., Lagarde, J., Dorothee, G. et al. (2016) Early and protective microglial activation in Alzheimer's disease: a prospective study using 18F-DPA-714 PET imaging. *Brain,* **139,** 1252-1264.

Hattori, N., Abe, K., Sakoda, S. and Sawada, T. (2002) Proton MR spectroscopic study at 3 Tesla on glutamate/glutamine in Alzheimer's disease. *Neuroreport,* **13,** 183-186.

Heneka, M. T., Carson, M. J., El Khoury, J. et al. (2015) Neuroinflammation in Alzheimer's disease. *Lancet Neurol,* **14,** 388-405.

Hiramatsu, M., Sasaki, M., Nabeshima, T. and Kameyama, T. (1997) Effects of dynorphin A (1-13) on carbon monoxide-induced delayed amnesia in mice. *Pharmacol Biochem Behav,* **56,** 73-79.

Huang, H., Nie, S., Cao, M., Marshall, C., Gao, J., Xiao, N., Hu, G. and Xiao, M. (2016) Characterization of AD-like phenotype in aged APPSwe/PS1dE9 mice. *Age (Dordr),* **38,** 303-322.

Jack, C. R., Jr., Marjanska, M., Wengenack, T. M., Reyes, D. A., Curran, G. L., Lin, J., Preboske, G. M., Poduslo, J. F. and Garwood, M. (2007) Magnetic resonance imaging of Alzheimer's pathology in the brains of living transgenic mice: a new tool in Alzheimer's disease research. *Neuroscientist,* **13,** 38-48.

James, M. L., Belichenko, N. P., Nguyen, T. V. et al. (2015) PET imaging of translocator protein (18 kDa) in a mouse model of Alzheimer's disease using N-(2,5-dimethoxybenzyl)-2-18F-fluoro-N-(2-phenoxyphenyl)acetamide. *J Nucl Med,* **56,** 311-316.

James, M. L., Fulton, R. R., Vercoullie, J. et al. (2008) DPA-714, a new translocator protein-specific ligand: synthesis, radiofluorination, and pharmacologic characterization. *J. Nucl. Med.,* **49,** 814-822.

Jankowsky, J. L., Fadale, D. J., Anderson, J. et al. (2004) Mutant presenilins specifically elevate the levels of the 42 residue beta-amyloid peptide in vivo: evidence for augmentation of a 42-specific gamma secretase. *Human molecular genetics,* **13,** 159-170.

Jansen, D., Zerbi, V., Janssen, C. I. et al. (2013) A longitudinal study of cognition, proton MR spectroscopy and synaptic and neuronal pathology in aging wild-type and AbetaPPswe-PS1dE9 mice. *PLoS One,* **8,** e63643.

Ji, B., Maeda, J., Sawada, M. et al. (2008) Imaging of peripheral benzodiazepine receptor expression as biomarkers of detrimental versus beneficial glial responses in mouse models of Alzheimer's and other CNS pathologies. *J Neurosci,* **28,** 12255-12267.

Johnson, G. A., Badea, A., Brandenburg, J., Cofer, G., Fubara, B., Liu, S. and Nissanov, J. (2010) Waxholm space: an image-based reference for coordinating mouse brain research. *Neuroimage,* **53,** 365-372.

Kantarci, K. (2007) 1H magnetic resonance spectroscopy in dementia. *The British journal of radiology,* **80 Spec No 2,** S146-152.

Kantarci, K., Weigand, S. D., Petersen, R. C. et al. (2007) Longitudinal 1H MRS changes in mild cognitive impairment and Alzheimer's disease. *Neurobiol Aging,* **28,** 1330-1339.

Klunk, W. E., Panchalingam, K., Moossy, J., McClure, R. J. and Pettegrew, J. W. (1992) N-acetyl-L-aspartate and other amino acid metabolites in Alzheimer's disease brain: a preliminary proton nuclear magnetic resonance study. *Neurology,* **42,** 1578-1585.

Knight, E. M., Martins, I. V., Gumusgoz, S., Allan, S. M. and Lawrence, C. B. (2014) High-fat diet-induced memory impairment in triple-transgenic Alzheimer's disease

(3xTgAD) mice is independent of changes in amyloid and tau pathology. *Neurobiol. Aging,* **35,** 1821-1832.

Kumar, A., Muzik, O., Shandal, V., Chugani, D., Chakraborty, P. and Chugani, H. T. (2012) Evaluation of age-related changes in translocator protein (TSPO) in human brain using (11)C-[R]-PK11195 PET. *J. Neuroinflammation,* **9,** 232.

Lee, Y., Oliynyk, S., Jung, J. C., Han, J. J. and Oh, S. (2013) Administration of glucosylceramide ameliorated the memory impairment in aged mice. *Evid Based Complement Alternat Med,* **2013,** 824120.

Liu, B., Le, K. X., Park, M. A. et al. (2015) In Vivo Detection of Age- and Disease-Related Increases in Neuroinflammation by 18F-GE180 TSPO MicroPET Imaging in Wild-Type and Alzheimer's Transgenic Mice. *J Neurosci,* **35,** 15716-15730.

Marjanska, M., Curran, G. L., Wengenack, T. M., Henry, P. G., Bliss, R. L., Poduslo, J. F., Jack, C. R., Jr., Ugurbil, K. and Garwood, M. (2005) Monitoring disease progression in transgenic mouse models of Alzheimer's disease with proton magnetic resonance spectroscopy. *Proc Natl Acad Sci U S A,* **102,** 11906-11910.

Marjanska, M., Weigand, S. D., Preboske, G. et al. (2014) Treatment effects in a transgenic mouse model of Alzheimer's disease: a magnetic resonance spectroscopy study after passive immunization. *Neuroscience,* **259,** 94-100.

Maroy, R., Boisgard, R., Comtat, C., Jego, B., Fontyn, Y., Jan, S., Dubois, A., Trebossen, R. and Tavitian, B. (2010) Quantitative organ time activity curve extraction from rodent PET images without anatomical prior. *Med Phys,* **37,** 1507-1517.

Maroy, R., Viel, T., Boisgard, R., Comtat, C., Trebossen, R. and Tavitian, B. (2008) Fast and accurate PET preclinical data analysis: segmentation and partial volume effect correction with no anatomical priors. *IEEE Nuclear Science Symposium Conference Record,* **M14,** 5498-5501.

Martins, I. V., Rivers-Auty, J., Allan, S. M. and Lawrence, C. B. (2017) Mitochondrial Abnormalities and Synaptic Loss Underlie Memory Deficits Seen in Mouse Models of Obesity and Alzheimer's Disease. *J Alzheimers Dis,* **55,** 915-932.

Mesholam, R. I., Moberg, P. J., Mahr, R. N. and Doty, R. L. (1998) Olfaction in neurodegenerative disease: a meta-analysis of olfactory functioning in Alzheimer's and Parkinson's diseases. *Arch Neurol,* **55,** 84-90.

Mhatre, S. D., Tsai, C. A., Rubin, A. J., James, M. L. and Andreasson, K. I. (2015) Microglial malfunction: the third rail in the development of Alzheimer's disease. *Trends Neurosci,* **38,** 621-636.

Mirzaei, N., Tang, S. P., Ashworth, S. et al. (2016) In vivo imaging of microglial activation by positron emission tomography with [(11)C]PBR28 in the 5XFAD model of Alzheimer's disease. *Glia,* **64,** 993-1006.

Murray, M. E., Przybelski, S. A., Lesnick, T. G. et al. (2014) Early Alzheimer's disease neuropathology detected by proton MR spectroscopy. *J. Neurosci.,* **34,** 16247-16255.

Nagakura, A., Shitaka, Y., Yarimizu, J. and Matsuoka, N. (2013) Characterization of cognitive deficits in a transgenic mouse model of Alzheimer's disease and effects of donepezil and memantine. *Eur J Pharmacol,* **703,** 53-61.

Oberg, J., Spenger, C., Wang, F. H. et al. (2008) Age related changes in brain metabolites observed by 1H MRS in APP/PS1 mice. *Neurobiol Aging,* **29,** 1423-1433.

Okello, A., Edison, P., Archer, H. A. et al. (2009) Microglial activation and amyloid deposition in mild cognitive impairment: a PET study. *Neurology,* **72,** 56-62.

Owen, D. R., Narayan, N., Wells, L. et al. (2017) Pro-inflammatory activation of primary microglia and macrophages increases 18 kDa translocator protein expression in rodents but not humans. *J Cereb Blood Flow Metab,* **37,** 2679-2690.

Papadopoulos, V., Lecanu, L., Brown, R. C., Han, Z. and Yao, Z. X. (2006) Peripheral-type benzodiazepine receptor in neurosteroid biosynthesis, neuropathology and neurological disorders. *Neuroscience,* **138,** 749-756.

Pardon, M. C., Yanez Lopez, M., Yuchun, D. et al. (2016) Magnetic Resonance Spectroscopy discriminates the response to microglial stimulation of wild type and Alzheimer's disease models. *Sci Rep,* **6,** 19880.

Parnetti, L., Tarducci, R., Presciutti, O., Lowenthal, D. T., Pippi, M., Palumbo, B., Gobbi, G., Pelliccioli, G. P. and Senin, U. (1997) Proton magnetic resonance spectroscopy can differentiate Alzheimer's disease from normal aging. *Mech Ageing Dev,* **97,** 9-14.

Perry, V. H. and Holmes, C. (2014) Microglial priming in neurodegenerative disease. *Nat. Rev. Neurol.,* **10,** 217-224.

Petrov, D., Pedros, I., Artiach, G. et al. (2015) High-fat diet-induced deregulation of hippocampal insulin signaling and mitochondrial homeostasis deficiences contribute to Alzheimer disease pathology in rodents. *Biochimica et biophysica acta,* **1852,** 1687-1699.

Ratiney, H., Sdika, M., Coenradie, Y., Cavassila, S., van Ormondt, D. and Graveron-Demilly, D. (2005) Time-domain semi-parametric estimation based on a metabolite basis set. *NMR Biomed,* **18,** 1-13.

Rose, S. E., de Zubicaray, G. I., Wang, D., Galloway, G. J., Chalk, J. B., Eagle, S. C., Semple, J. and Doddrell, D. M. (1999) A 1H MRS study of probable Alzheimer's disease and normal aging: implications for longitudinal monitoring of dementia progression. *Magn Reson Imaging,* **17,** 291-299.

Rubio-Perez, J. M. and Morillas-Ruiz, J. M. (2012) A review: inflammatory process in Alzheimer's disease, role of cytokines. *TheScientificWorldJournal,* **2012,** 756357.

Scarf, A. M. and Kassiou, M. (2011) The translocator protein. *J. Nucl. Med.,* **52,** 677-680.

Schuitemaker, A., Kropholler, M. A., Boellaard, R. et al. (2013) Microglial activation in Alzheimer's disease: an (R)-[(1)(1)C]PK11195 positron emission tomography study. *Neurobiol. Aging,* **34,** 128-136.

Serriere, S., Tauber, C., Vercouillie, J. et al. (2015) Amyloid load and translocator protein 18 kDa in APPswePS1-dE9 mice: a longitudinal study. *Neurobiol Aging,* **36,** 1639-1652.

Shiino, A., Watanabe, T., Shirakashi, Y., Kotani, E., Yoshimura, M., Morikawa, S., Inubushi, T. and Akiguchi, I. (2012) The profile of hippocampal metabolites differs between Alzheimer's disease and subcortical ischemic vascular dementia, as measured by proton magnetic resonance spectroscopy. *J Cereb Blood Flow Metab,* **32,** 805-815.

Shinno, H., Inagaki, T., Miyaoka, T., Okazaki, S., Kawamukai, T., Utani, E., Inami, Y. and Horiguchi, J. (2007) A decrease in N-acetylaspartate and an increase in myoinositol in the anterior cingulate gyrus are associated with behavioral and psychological symptoms in Alzheimer's disease. *J Neurol Sci,* **260,** 132-138.

Song, C., Zhang, Y. and Dong, Y. (2013) Acute and subacute IL-1beta administrations differentially modulate neuroimmune and neurotrophic systems: possible implications for neuroprotection and neurodegeneration. *J Neuroinflammation,* **10,** 59.

Stalder, M., Phinney, A., Probst, A., Sommer, B., Staufenbiel, M. and Jucker, M. (1999) Association of microglia with amyloid plaques in brains of APP23 transgenic mice. *Am J Pathol,* **154,** 1673-1684.

Stefan, D., Di Cesare, F., Andrasescu, A. et al. (2009) Quantitation of magnetic resonance spectroscopy signals: the jMRUI software package. *Measurement Science and Technology,* **20,** 104035.

Swardfager, W., Lanctot, K., Rothenburg, L., Wong, A., Cappell, J. and Herrmann, N. (2010) A meta-analysis of cytokines in Alzheimer's disease. *Biol Psychiatry,* **68,** 930-941.

Takkinen, J. S., Lopez-Picon, F. R., Al Majidi, R. et al. (2016) Brain energy metabolism and neuroinflammation in ageing APP/PS1-21 mice using longitudinal 18F-FDG and 18F-DPA-714 PET imaging. *J. Cereb. Blood Flow Metab.*, 271678X16677990.

Turkheimer, F. E., Edison, P., Pavese, N. et al. (2007) Reference and target region modeling of [11C]-(R)-PK11195 brain studies. *J. Nucl. Med.,* **48,** 158-167.

Urenjak, J., Williams, S. R., Gadian, D. G. and Noble, M. (1993) Proton nuclear magnetic resonance spectroscopy unambiguously identifies different neural cell types. *J Neurosci,* **13,** 981-989.

van den Boogaart, A., van Ormondt, D., Pijnappel, W. W. F., de Beer, R. and Ala Korpel, M. (1994) Removal of the residual water resonance from 1H magnetic resonance spectra. . *Mathematics of Signal Processing III, Clarendon Press: Oxford,* 175-195.

van Groen, T., Kiliaan, A. J. and Kadish, I. (2006) Deposition of mouse amyloid beta in human APP/PS1 double and single AD model transgenic mice. *Neurobiol Dis,* **23,** 653-662.

Varnum, M. M. and Ikezu, T. (2012) The classification of microglial activation phenotypes on neurodegeneration and regeneration in Alzheimer's disease brain. *Arch. Immunol. Ther. Exp. (Warsz.),* **60,** 251-266.

Varrone, A. and Lammertsma, A. A. (2015) Imaging of neuroinflammation: TSPO and beyond. *Clin. Transl. Imaging,* **3,** 389-390.

Varrone, A., Mattsson, P., Forsberg, A. et al. (2013) In vivo imaging of the 18-kDa translocator protein (TSPO) with [18F]FEDAA1106 and PET does not show increased binding in Alzheimer's disease patients. *Eur J Nucl Med Mol Imaging,* **40,** 921-931.

Varrone, A., Oikonen, V., Forsberg, A. et al. (2015) Positron emission tomography imaging of the 18-kDa translocator protein (TSPO) with [18F]FEMPA in Alzheimer's disease patients and control subjects. *Eur J Nucl Med Mol Imaging,* **42,** 438-446.

Venneti, S., Lopresti, B. J., Wang, G., Hamilton, R. L., Mathis, C. A., Klunk, W. E., Apte, U. M. and Wiley, C. A. (2009) PK11195 labels activated microglia in Alzheimer's disease and in vivo in a mouse model using PET. *Neurobiol. Aging,* **30,** 1217-1226.

von Kienlin, M., Kunnecke, B., Metzger, F., Steiner, G., Richards, J. G., Ozmen, L., Jacobsen, H. and Loetscher, H. (2005) Altered metabolic profile in the frontal cortex of PS2APP transgenic mice, monitored throughout their life span. *Neurobiol Dis,* **18,** 32-39.

Watanabe, T., Shiino, A. and Akiguchi, I. (2010) Absolute quantification in proton magnetic resonance spectroscopy is useful to differentiate amnesic mild cognitive impairment from Alzheimer's disease and healthy aging. *Dement Geriatr Cogn Disord,* **30,** 71-77.

Webster, S. J., Bachstetter, A. D. and Van Eldik, L. J. (2013) Comprehensive behavioral characterization of an APP/PS-1 double knock-in mouse model of Alzheimer's disease. *Alzheimer's research & therapy,* **5,** 28.

Wesson, D. W., Borkowski, A. H., Landreth, G. E., Nixon, R. A., Levy, E. and Wilson, D. A. (2011) Sensory network dysfunction, behavioral impairments, and their reversibility in an Alzheimer's beta-amyloidosis mouse model. *J Neurosci,* **31,** 15962-15971.

Westin, K., Buchhave, P., Nielsen, H., Minthon, L., Janciauskiene, S. and Hansson, O. (2012) CCL2 is associated with a faster rate of cognitive decline during early stages of Alzheimer's disease. *PLoS One,* **7,** e30525.

Wiley, C. A., Lopresti, B. J., Venneti, S., Price, J., Klunk, W. E., DeKosky, S. T. and Mathis, C. A. (2009) Carbon 11-labeled Pittsburgh Compound B and carbon 11-labeled (R)-PK11195 positron emission tomographic imaging in Alzheimer disease. *Arch. Neurol.,* **66,** 60-67.

Xiong, H., Callaghan, D., Wodzinska, J., Xu, J., Premyslova, M., Liu, Q. Y., Connelly, J. and Zhang, W. (2011) Biochemical and behavioral characterization of the double transgenic mouse model (APPswe/PS1dE9) of Alzheimer's disease. *Neurosci Bull,* **27,** 221-232.

Xu, W., Zhan, Y., Huang, W., Wang, X., Zhang, S. and Lei, H. (2010) Reduction of hippocampal N-acetyl aspartate level in aged APP(Swe)/PS1(dE9) transgenic mice is associated with degeneration of CA3 pyramidal neurons. *J Neurosci Res,* **88,** 3155-3160.

Yang, D., Xie, Z., Stephenson, D. et al. (2011) Volumetric MRI and MRS provide sensitive measures of Alzheimer's disease neuropathology in inducible Tau transgenic mice (rTg4510). *Neuroimage,* **54,** 2652-2658.

Yao, Z. G., Jing, H. Y., Wang, D. M. et al. (2016) Valproic acid ameliorates olfactory dysfunction in APP/PS1 transgenic mice of Alzheimer's disease: Ameliorations from the olfactory epithelium to the olfactory bulb. *Pharmacol Biochem Behav,* **144,** 53-59.

Yokokura, M., Mori, N., Yagi, S. et al. (2011) In vivo changes in microglial activation and amyloid deposits in brain regions with hypometabolism in Alzheimer's disease. *Eur. J. Nucl. Med. Mol. Imaging,* **38,** 343-351.

Yokokura, M., Terada, T., Bunai, T. et al. (2017) Depiction of microglial activation in aging and dementia: Positron emission tomography with [11C]DPA713 versus [11C](R)PK11195. *J Cereb Blood Flow Metab,* **37,** 877-889.

Zhang, W., Bai, M., Xi, Y., Hao, J., Liu, L., Mao, N., Su, C., Miao, J. and Li, Z. (2012) Early memory deficits precede plaque deposition in APPswe/PS1dE9 mice: involvement of oxidative stress and cholinergic dysfunction. *Free Radic Biol Med,* **52,** 1443-1452.

List of abbreviations

AD	Alzheimer's disease
Aβ	β-amyloid plaques
CD11b	integrin αM chain of the Macrophage-1 antigen
CSF	cerebrospinal fluid
Cr	creatine & phosphocreatine
DI	discrimination index
Tf	Time spent exploring the familiar object/scent
GFAP	Glial fibrillary acidic protein
Glu	glutamate
MRS	magnetic resonance spectroscopy
MAP2	Microtubule-associated protein-2
MCI	mild cognitive impairment
MR	magnetic resonance
mI	myo-inositol

NAA	N-acetylaspartate
NFTs	neurofibrillary tangles
NUVcb	normalised (to the cerebellum) uptake value
NOR	novel object recognition
NSR	Novel smell recognition
PET	positron emission tomography
SUV	standard uptake value
SVA2	Synaptic vesicle glycoprotein 2A
Taur	taurine
Tn	time spent exploring the novel object/scent
tCho	total choline
T	total time exploring objects/scents
TG	Transgenic
TSPO	translocator receptor 18kDa
WT	wild type

Figure Legends

Figure 1: Gantt chart of the study. Behaviour tests and PET and MRS scans were performed at 6, 12 and 18 months of age. Behaviour tests were also performed at two additional time-points to evaluate potential cognitive changes and would cognitive deficit been detected at 9 months the imaging time-points would have been brought forward.

Figure 2: Discrimination index (DI) of exploration of the novel and the familiar object (**a**) and smell (**c**) in phase 1 and 2 (WT n=11, TG=15 at 6 months, WT n=6, TG=9 at 12 months, WT n=6, TG=6 at 18 months). Exploration times of right and left objects in phase 1 of the NOR (**b**) and NSR (**d**) (*t*-tests per genotype at each age). Time spent in the presence of predator and non-predator urine (n=4) (**e**). Alternation in the Y-maze (WT n=16, TG=18 at 6 months, WT=12, TG=11 at 12 months, WT=9, TG=10 at 18 months) (**f**). Results are shown as mean±SEM. Statistical analysis was performed using two-way ANOVAs and Sidak's multiple comparisons post-hoc tests (***p≤0.001).

Figure 3: PET images showing [^{18}F]DPA-714 uptake in WT and APP_{swe}×$PS1_{\Delta e9}$ mice at 6 (WT n=10, TG=7), 12 (WT n=8, TG=9) and 18 months (WT n=10, TG=9) of age (**a**). NUV_{cb} values in the hippocampus and cortex (**b**) and other subcortical regions (**c**). Results are expressed as mean±SD. Statistical analysis was performed using two-way ANOVA followed by Sidak's and Dunnet's post-hoc analysis (*p≤0.05, **p≤0.01).

Figure 4: Example spectra from WT and TG mice at 6, 12 and 18 months (**a**). Metabolites expressed as ratios to creatine in WT (n=6) (**b**) and TG (n=8) (**c**) mice at 6, 12 and 18 months of age. No differences were observed in the Cr concentration (mean±SD) referenced to water (**d**). Reduced Glu/Cr and increased tCho levels were observed with age in both WT and TG (independently of genotype). Results are shown as mean±SD. Statistical analysis was performed using two-way ANOVA followed by Dunnet's *post hoc* analysis. (****p≤0.0001).

Figure 5: Immunoreactivity of GFAP (green) and CD11b (red). Representative images of double staining in the hippocampus (**a**) and cortex (**b**) of WT and APP_{swe}×$PS1_{\Delta e9}$ mice at 6, 12 and 18 months of age. Pictures were taken at 10× magnification between bregma -2.06mm and -2.30mm. Scale bar represents 200µm.

Figure 6: Immunoreactivity of TSPO (green) and CD11b (red). Representative images of double staining in the hippocampus (**a**) and cortex (**b**) of WT and APP_{swe}×$PS1_{\Delta e9}$ mice at 6, 12 and 18 months of age. Pictures were taken at 10× magnification between bregma -2.06mm and -2.30mm. Scale bar represents 200µm.

Figure 7: Immunoreactivity of TSPO (green) and Aβ (red). Representative images of double staining in the hippocampus (**a**) and cortex (**b**) of WT and APP_{swe}×$PS1_{\Delta e9}$ mice at 6, 12 and 18 months of age. Pictures were taken at 10× magnification between bregma -2.06mm and -2.30mm. Scale bar represents 200µm.

Figure 8: Immunoreactivity of MAP2 (green) and NeuN (red). Representative images of double staining in the hippocampus (**a**) and cortex (**b**) of WT and APP_{swe}×$PS1_{\Delta e9}$ mice at 6, 12 and 18 months of age. Pictures were taken at 10× magnification between bregma -2.06mm and -2.30mm. Scale bar represents 200µm.

Figure 9: Immunoreactivity of neurogranin (red) and SV2A (green). Representative images of single SVA2 staining in the hippocampus (**a**) and cortex (**b**) and neurogranin staining in the hippocampus (**c**) and cortex (**d**) of WT and APP_{swe}×$PS1_{\Delta e9}$ mice at 6, 12 and 18 months of age. Pictures were taken at 10× magnification between bregma -2.06mm and -2.30mm. Scale bar represents 200µm.

Supplementary figure 1: Whole brain was segmented into the hippocampus and cortex (**a**), other subcortical (**b**) and cerebellum (**c**) regions of interest for PET quantification using a modified version of the Waxholm space template (Johnson et al. 2010). The MRS voxel was centred at bregma -2.30mm according to the Paxinos mouse brain atlas and encompassed hippocampal and thalamic regions (**d**). Example of an MRS spectrum i*n vivo* with the main metabolites highlighted (**e**). AAP-amino acid proton, mI-myo-Inositol. Tau-taurine, Cho-choline containing compounds, Cre- creatine+phosphocreatine, Glu- glutamate, GABA- γ-aminobutyric acid, NAA- N-acetylaspartate, Lipid MMS- lipid and macromolecules.

Supplementary figure 2: [^{18}F]DPA-714 standard uptake value in the cerebellum of WT and APPswe×PS1Δe9 mice at 6 (WT n=10, TG=7), 12 (WT n=8, TG=9) and 18 months (WT n=10, TG=9) of age. Results are expressed as mean±SD. Statistical analysis was performed using two-way ANOVA followed by Sidak's post-hoc analysis (*p≤0.05).

Supplementary figure 3: Immunoreactivity of GFAP (green) and CD11b (red). Representative images of double staining in the hippocampus (**a**) and cortex (**b**) of WT and APP_{swe}×$PS1_{\Delta e9}$ mice at 6, 12 and 18 months of age. Pictures were taken at **20×** magnification between bregma -2.06mm and -2.30mm. Scale bar represents 200µm.

Supplementary figure 4: Immunoreactivity of TSPO (green) and CD11b (red). Representative images of double staining in the hippocampus (a) and cortex (b) of WT and APPswe×PS1Δe9 mice at 6, 12 and 18 months of age. Pictures were taken at **20×** magnification between bregma -2.06mm and -2.30mm. Scale bar represents 200µm.

Supplementary figure 5: Immunoreactivity of MAP2 (green) and NeuN (red). Representative images of double staining in the hippocampus (**a**) and cortex (**b**) of WT and APP_{swe}×$PS1_{\Delta e9}$

mice at 6, 12 and 18 months of age. Pictures were taken at **20×** magnification between bregma -2.06mm and -2.30mm. Scale bar represents 200µm.

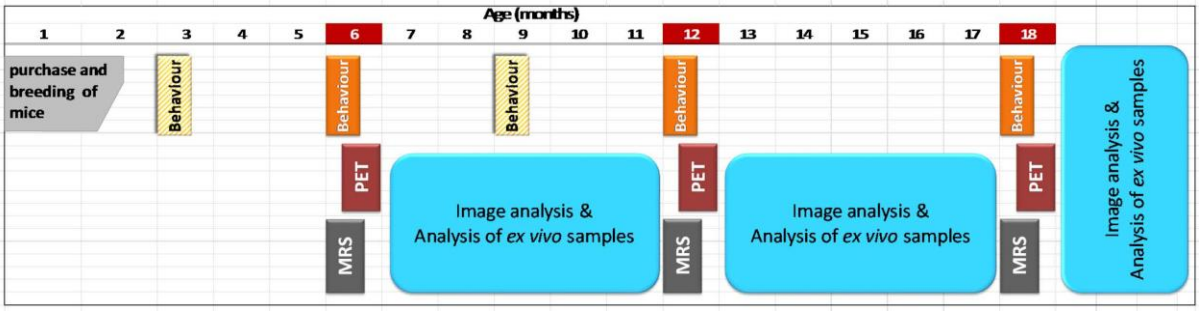

Figure 1

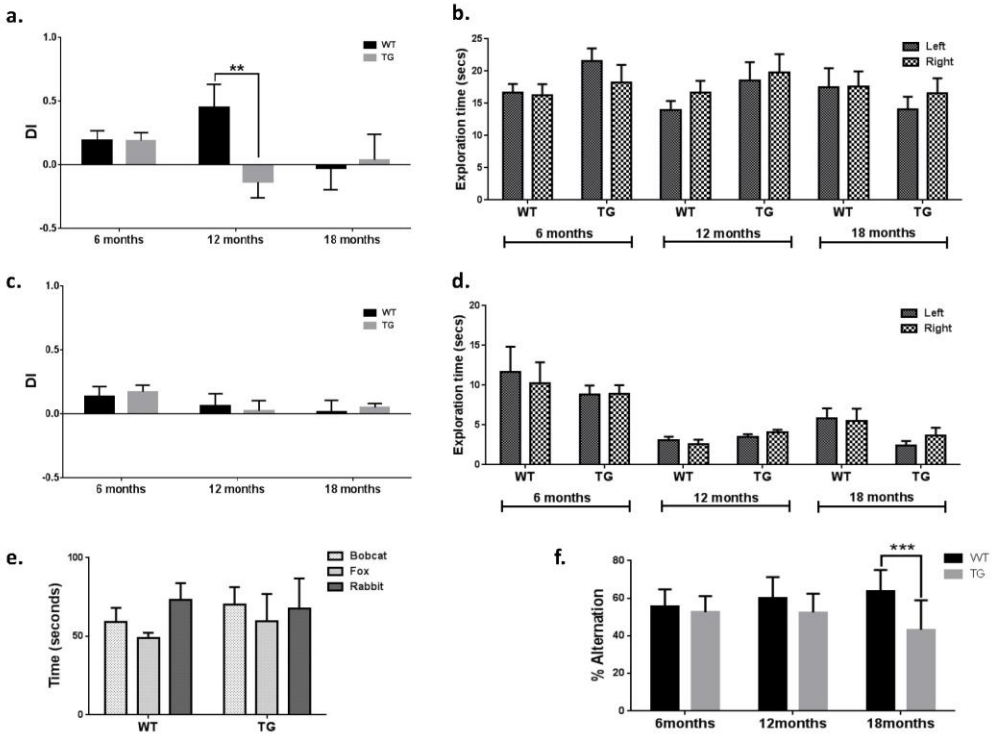

Figure 2

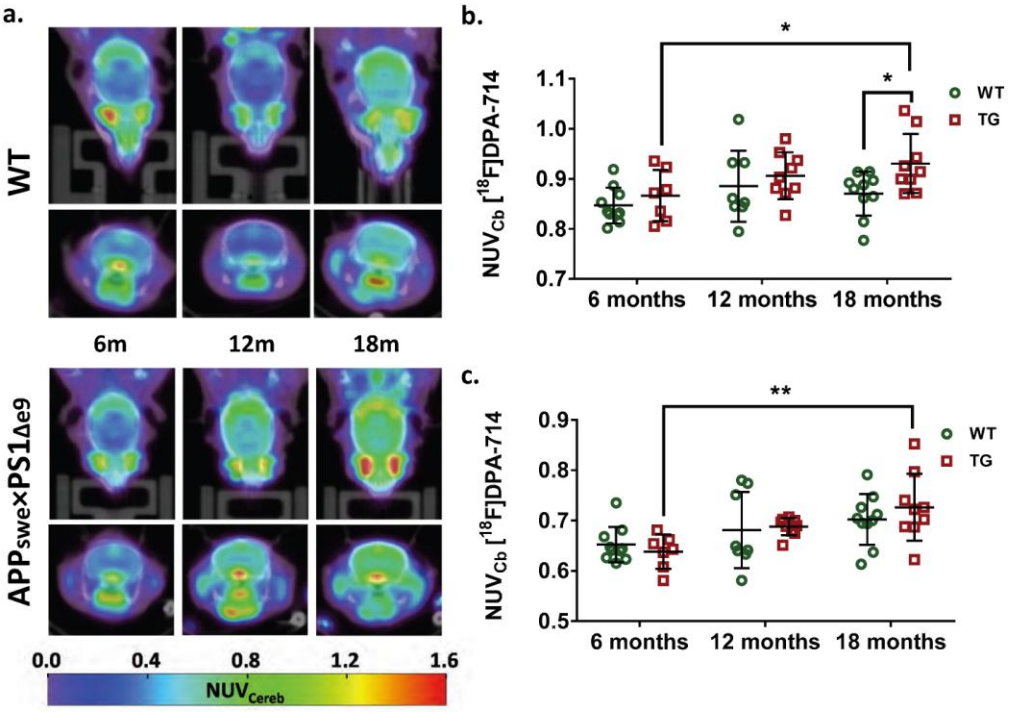

Figure 3

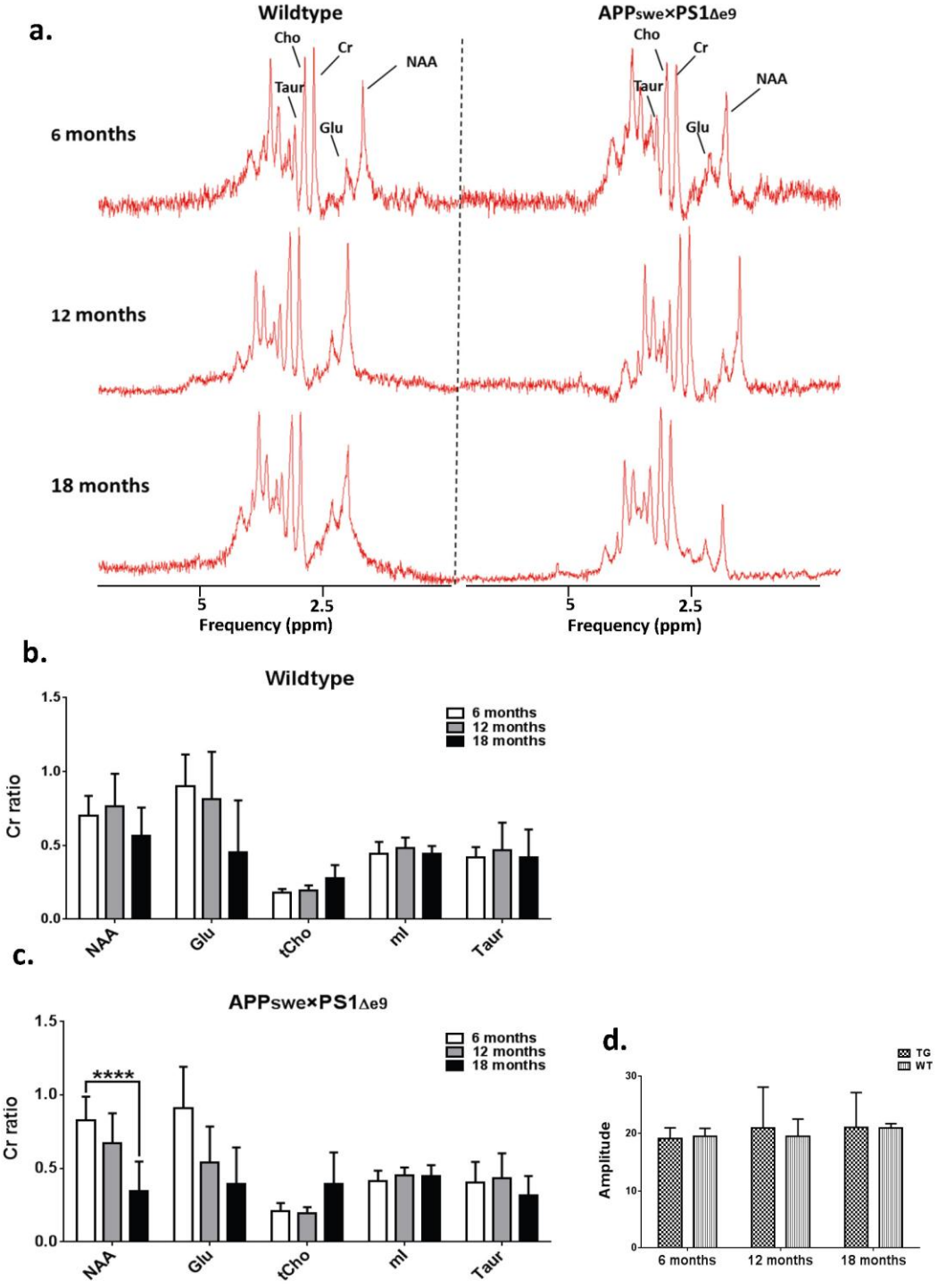

Figure 4

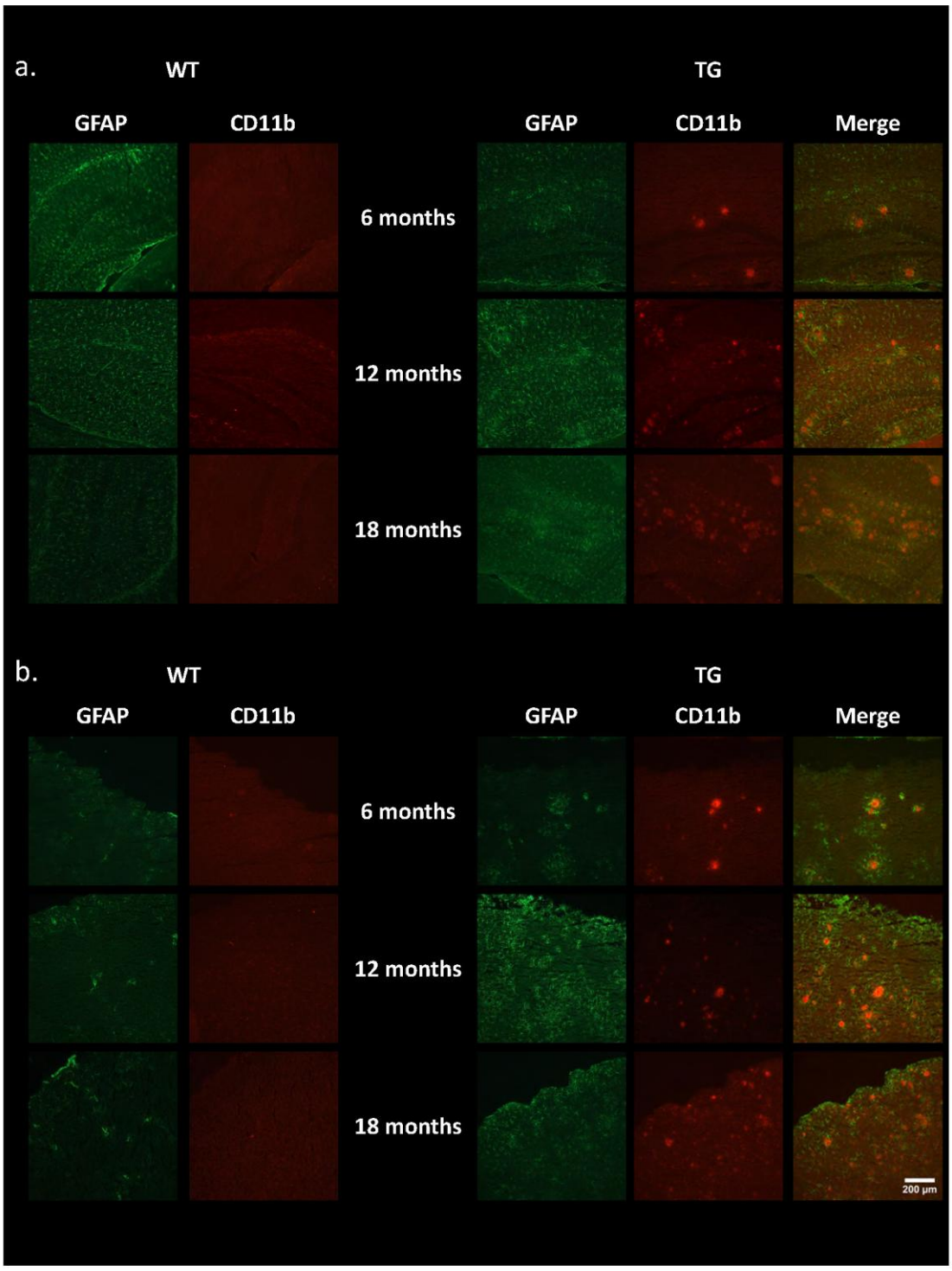

Figure 5

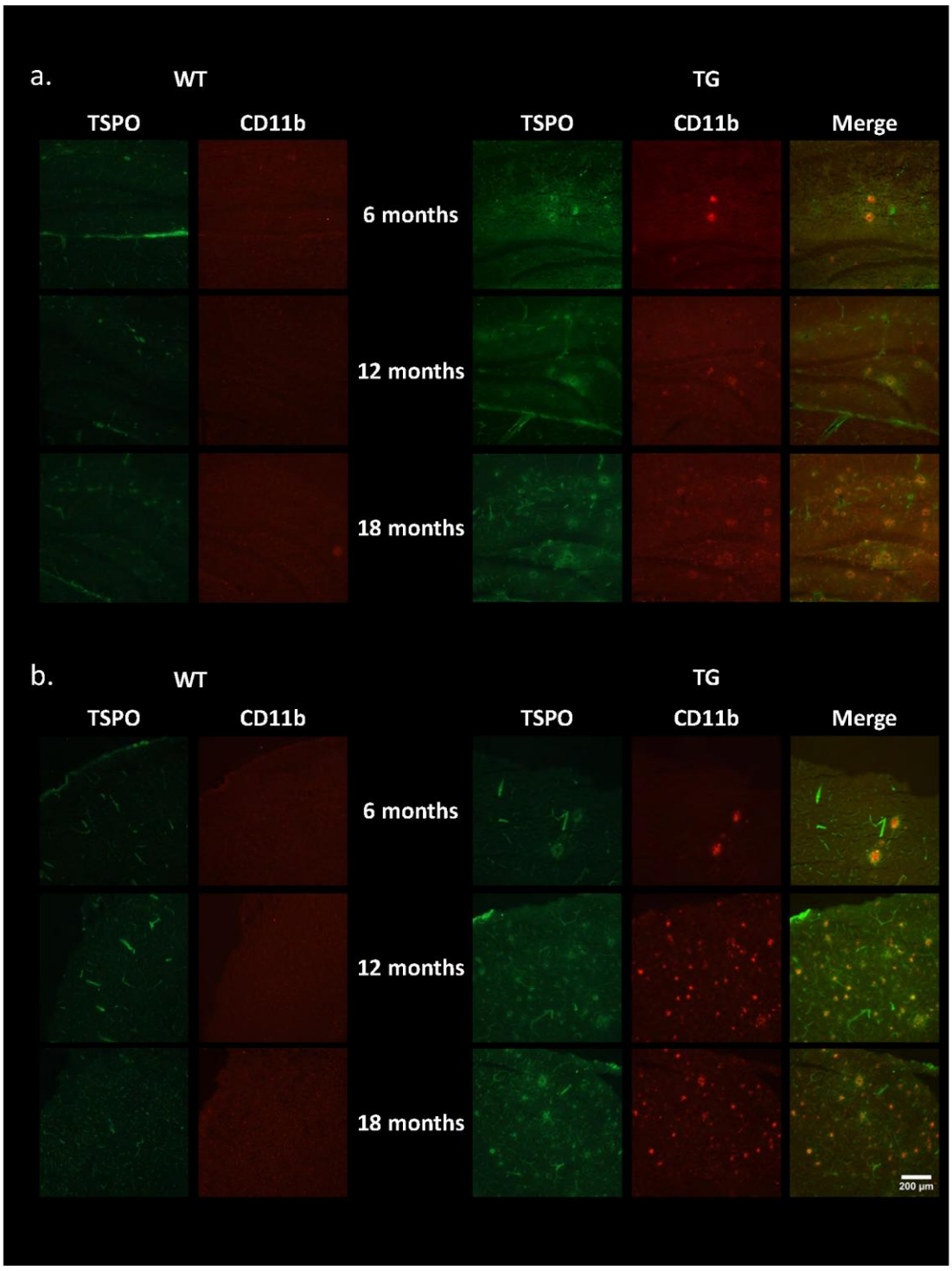

Figure 6

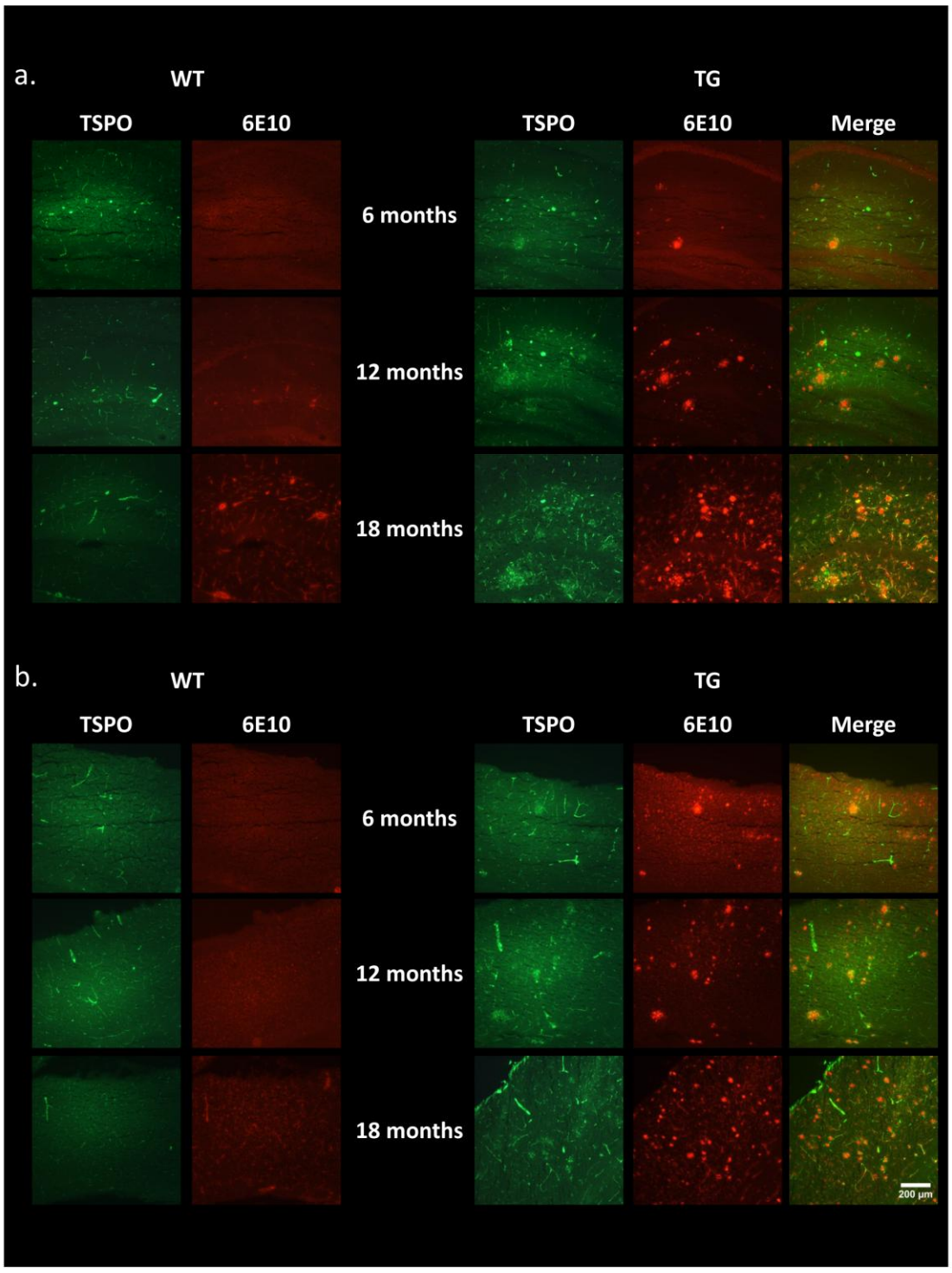

Figure 7

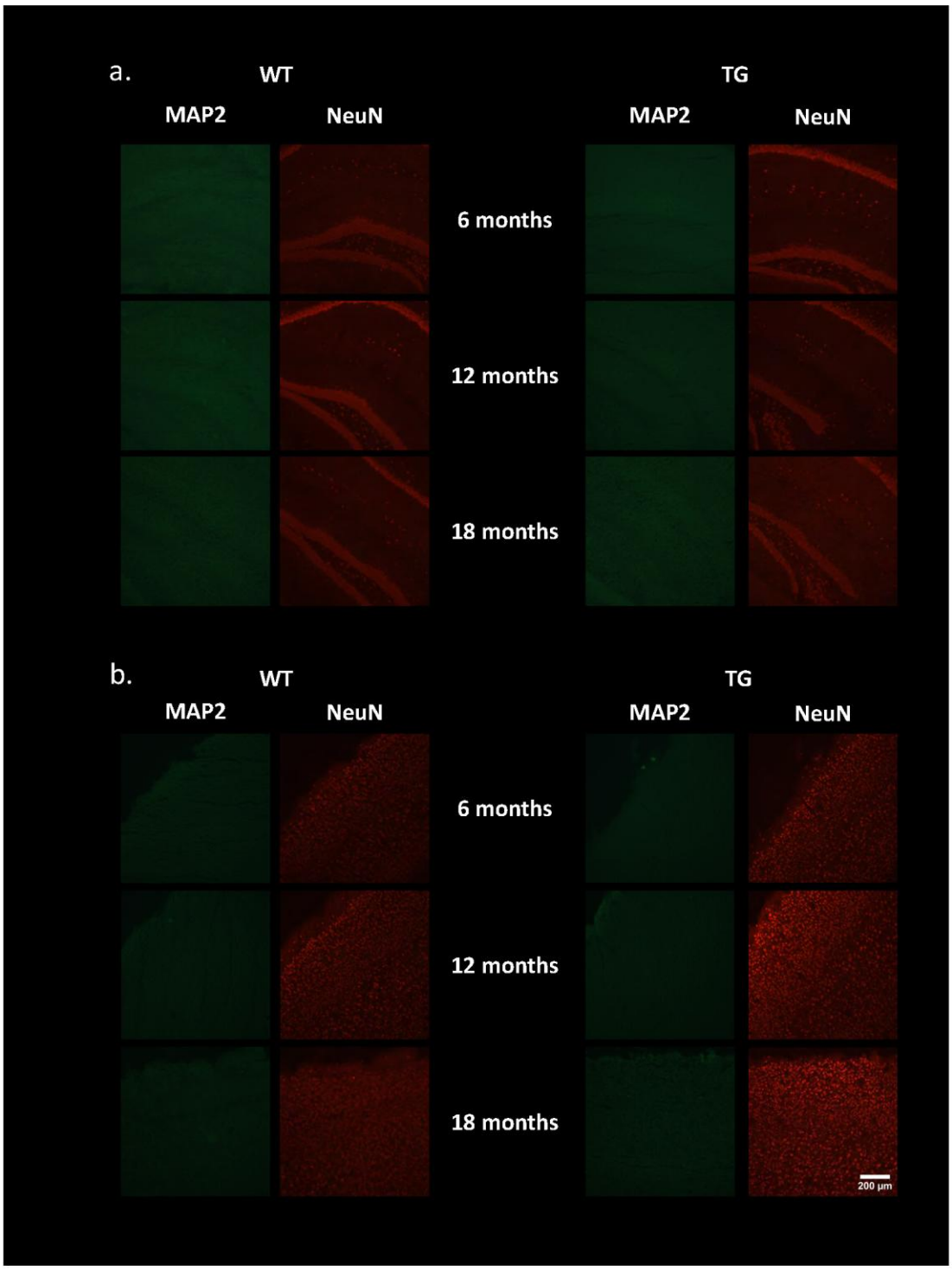

Figure 8